An *in vivo* CRISPR screen unveils top target genes to improve CAR-T cell efficacy in a solid tumor model

Mattia Fumagalli[1,2,3*], Dongjie An[1,2], Luca Simula[1,2], Camille Combe[1,2], Lisa Aziez[1], Yannick Simoni[1], Marie-Clotilde Alves-Guerra[1], Andrea Valentini[4], Maude Marchais[1], Anaïs Vermare[1,2], Josquin Moraly[5], Nadège Bercovici[1,2], Emmanuel Donnadieu[1,2] and Frédéric Pendino[1,2*]

[1] Université Paris Cité, Institut Cochin, INSERM, CNRS, F-75014 Paris, France
[2] Equipe Labélisée Ligue Nationale Contre le Cancer
[3] Thèse financée par la Ligue Nationale Contre le Cancer
[4] Technical University of Denmark, 2800 Kgs. Lyngby, Denmark
[5] Pediatric Oncology Branch, National Cancer Institute, National Institutes of Health, Bethesda, MD, USA

* Correspondence: frederic.pendino@inserm.fr and mattia.fumagalli@inserm.fr

ABSTRACT

CAR-T cell therapies are revolutionizing the treatment of refractory and relapsed haematological malignancies, but many patients do not exhibit long-term responses, and these therapies are less effective against solid tumors. Poor persistence of CAR-T cells in patients is associated with therapeutic failure, highlighting the need to identify strategies promoting *in vivo* expansion. Here, we developed an *in vivo* competitive screening method to identify genes whose inactivation confers a selective advantage to CAR-T cells. Inactivation of 50 genes in a heterogeneous population of T cells expressing an EGFR-targeting CAR revealed that disruption of *REGNASE-1, SOCS1, PTPN2*, and *P16INK4A* conferred a selective advantage to CAR-T cells in human lung tumor-bearing mice. Consistently, inactivation of these genes improved tumor eradication by CAR-T cells. Interestingly disruption of other genes, described to improve CAR-T cell function in other contexts, had a negative impact in this orthotopic lung tumor model. Further evaluation of long-term effects in a subcutaneous model, highlighted *SOCS1* ablation as the most promising strategy for *in vivo* CAR-T cell amelioration. These results support the importance of evaluating CAR-T cell editing strategies in tumor-specific models and highlight the versatility of our screening approach as a pre-clinical tool for context-specific studies on CAR-T cells amelioration.

INTRODUCTION

Chimeric Antigen Receptor (CAR) T cells are emerging as an effective treatment for highly refractory and relapsed haematological malignancies, such as leukaemia, lymphomas, and myeloma. Yet, an important fraction of patients still does not respond to these treatments, and despite recent encouraging successes, CAR-T therapy efficacy remains limited in most solid tumors[1]. Clinical trials in leukaemia and lymphomas have shown that a poor expansion and persistence of CAR-T cells in the patient are the main factors predicting a poor prognostic outcome[2]. Coherently, unsuccessful first clinical trials of CAR-T cells against solid tumors report very low numbers of CAR-T cells in patients [3, 4]. On the contrary in different successful clinical trials of CAR-T against solid tumors, [5] especially for anti-GD2 CAR-T cells or anti-IL13Ralpha2 in glioblastoma, CAR-T proliferation and persistence in responding patients were comparable to those of successful anti-CD19 CAR-T therapies, correlating with clinical efficacy[6, 7]. Such results indicate that also in solid tumors, where other obstacles limit their efficacy, a good proliferation and persistence of CAR-T cells remain ultimately essential[4, 8].

Amelioration of CAR-T cells therapy is currently being pursued through several strategies and gene editing approaches are among the most promising.[8-10] Growing number of studies have shown that the ablation of some genes, encoding transcription (co)factors (*IKFZ3, BATF*...)[11, 12], epigenetic modulators (*DNMT3A, TET2*...)[13, 14], signaling regulators (*SOCS1*, DGK-alpha/zeta...)[15, 16], or immunomodulatory receptors (*PD1, TIM3*...)[17, 18], could result in improvement of T or CAR-T cell efficacy, with enhanced expansion or persistence in some *in vitro* or *in vivo* preclinical models. Such results are really promising, but they have been obtained in different experimental conditions, in terms of CAR structure, target antigen, manufacture protocol or tumor model. Since all these elements have been proven to influence CAR-T cell efficacy, it is impossible to directly compare the effects of these different gene candidates[19-23].

Whole genome CRISPR screenings somehow compare the effect of several gene KO simultaneously, such approaches have been successfully applied for in studies on T or CAR-T cells, allowing discovery of new potential candidates target genes[24-30]. Nonetheless, results are not very consistent among these different screenings, suggesting the need for context-specific analyses, in relevant preclinical models. Unfortunately, experiments constraints, such as poor infiltration in tumor tissues or reduced in situ proliferation, pose challenges in *in vivo* solid cancer models[31]. As a result, whole genome approaches would be hardly applicable for specific studies on given CAR-T cells in specific tumor contexts. Notably, large gRNA libraries used in such screenings generally force tailored experimental settings, with expensive and time-consuming sequencing pipelines[27, 28].

Here, we propose a new versatile pre-clinical tool to directly evaluate simultaneously the impact of 50 selected gene modifications in CAR-T cells, through a re-purposing of the CRISPR-KO screening approach. Through this work, we report the application of this strategy to improve CAR-T cells in models of non-small cells lung adenocarcinoma, a promising yet challenging solid tumor target for CAR-T therapy development[32, 33].

RESULTS

Set up of a CRISPR-Cas9 system to edit 50 top target genes in a pool of CAR-T cells and a method to quantify subpopulations of edited CAR-T

By an extensive search in the literature in march 2023, we defined a list of 50 genes whose inactivation in T or CAR-T cells could increase their proliferation, persistence or long-term efficiency[11-18, 24-30, 34-66]. (Fig 1 A, Tab. 1) Then, we set up a method to integrate gene editing in the production pipeline of second generation 4-1BB CAR-T cells targeting EGFR. By using a bank of lentiviral vectors expressing a total of 236 gRNAs (4 guides per gene, including 4 negative control genes and 20 non-targeting guides), and transient nucleofection of the Cas9 protein, we produced a pool of CAR-T cells carrying inactivating mutations in one of the selected genes. (Fig. 1 A, B). First, we validated this editing system, successfully targeting *Enhanced Green Fluorescent Protein* gene (*EGFP*) (Fig 1 C). Then, we tested the editing of a gene encoding an epigenetic factor, *RINF*, for which we confirmed effective editing at a genomic level by Tracking of Indels by Decomposition (TIDE) assay (Fig 1 D).

Then, we produced the lentiviral vectors library and set up quantification of CAR-T Knockout (KO) subpopulations by targeted Next Generation Sequencing (NGS). Data were analyzed through Model-based Analysis of Genome-wide CRISPR-Cas9 Knockout (MAGeCK) a bioinformatic tool for gene ranking according to sgRNAs frequencies.[6]
We validated the efficiency of our library by assessing the impact of sgRNA targeting T cell activation genes, previously defined as essential in whole genome CRISPR-KO studies.[24, 26] CAR-T cells inactivated for these genes, *RHOH, LCP2, VAV1* and *ZAP70,* are all significantly negatively selected upon anti-CD3/CD28 driven *in vitro* expansion of CAR-T cells (Fig 1 E,F). Interestingly some candidate genes in this screening are well known negative regulators of T cells activation, and among them KOs of *CBL-B, CD5, DGK-Z, RASA2* were significantly positively selected (Fig 1 F). These results validated our editing system, the lentiviral bank as well as the targeted NGS sequencing strategy and bioinformatic pipeline employed for the analysis.

Set up and validation of a relevant in vivo orthotopic tumor model of CAR-T therapy

To start, we confirmed that T cells transduced with the 4-1BB anti-EGFR CAR construct efficiently and specifically target EGFR-expressing tumor cells. (Supplementary Fig. 1 A, B) The EGFR antigen is expressed by different solid tumors, including the A549 lung adenocarcinoma cell line. We used this cell line to establish an orthotopic model of lung tumor in immunocompromised NSG mice. (Fig. 2 A, B, C). We observed that our CAR-T cells can infiltrate and accumulate in tumor islets, (Fig. 2 B, Supplementary fig. 1 C) and specifically control and eradicate tumors. (Fig. 2 D). We could isolate CAR-T cells from mice lung at the experiment's endpoint and observed the upregulation of differentiation, activation, and exhaustion markers (Fig. 2 E, Supplementary fig. 1 D). Coherently, such cells show reduced cytotoxicity and proliferation indicating that tumor exposure in this model can induce dysfunction in CAR-T cells (Fig. 2 F).

Interestingly, by gathering data from different experiments, we could observe a strong inverse correlation between the tumour charge and CAR-T cells number in mice lung at the endpoint of the experiment (Fig. 2 G). Such relation appears stronger than an inverse linear correlation, and could instead be described by a power law, as we demonstrated by statistical data fitting (Fig. 2 G). Such

observation confirms a strong relationship between CAR-T cell persistence/proliferation and tumor progression in this model.

Overall, these findings support the relevance of this orthotopic lung tumor model for the proposed study.

The In vivo CRISPR-KO screening assay allows to distinguish, among 50 top candidate genes, those whose KO gives the clearest selective in vivo advantage to CAR-T cells

To identify the best target genes to improve CAR T expansion and *in vivo* persistence, we injected tumor-bearing mice with CAR-T cells modified with our lentiviral bank (Fig. 3 A). To increase the power of the test, we produced CAR-T cells from the blood of three healthy donors and we defined sub-optimal therapy conditions, allowing tumor control but not total eradication, for at least five weeks (Fig. 3 B). At the endpoint of the experiments, we could detect substantial proportions of CAR-T in the lungs (Fig. 3 C), which allowed us to quantify each sub-population of the pool of edited CAR-T cells. Briefly, from DNA extracts of the tumor bearing mice lungs, we amplified the sgRNA expressing region of lentiviral vectors in CAR-T cells. PCR amplicons underwent NGS sequencing and data were analyzed with MAGeCK, algorithm.

In tumor samples, most of sgRNAs could be detected, even in samples with very low CAR-T cells numbers, proving the good sensitivity of our approach (Supplementary fig. 2 A). We could then define gene targets significantly enriched in different tumor samples of mice receiving CAR-T cells from each blood donor. (Fig. 3 D)
Most importantly, we could detect that sgRNA for the KO of the genes *REGNASE-1, SOCS1, PTPN2 and P16INK4A*, led to a robust selective advantage of CAR-T cells consistently among the three different donors. (Fig. 3 E) As expected we observed depletion of KO of essential genes of the TCR-signaling, used as negative controls. Surprisingly though, some target genes for CAR-T cell amelioration, notably *MED12, PRDM1* and *BATF,* scored as bad or even worse. These genes, while increasing CAR-T cell proliferation or persistence in the experimental conditions of the respective studies,[11, 26, 50] appear rather to impair such capabilities in these specific experimental conditions. (Fig. 3 E).

Throughout the setting up of such screening, different experiments on CAR-T cells from the same donors were performed. We observed that in conditions where CAR-T cells rapidly eradicated tumors, and therefore underwent minimal selective pressure, no meaningful effect could be observed in term of gene-ko subpopulations selection. (Fig. 3 F left, Supplementary fig. 2 B) In more stringent conditions, however, we observed more pronounced effects on gene-ko subpopulations enrichment (Fig. 3 F middle and right, Supplementary fig. 2 B), proving that these outcomes were strictly dependent on selective pressure and are specific to CAR-T cells exposure to tumor.

Overall, these screening results demonstrate the feasibility of our approach and strongly support the value of assessing the effects of gene-editing strategies on specific CAR-T cells and contexts, using models that closely mimic clinical settings.

186 ***Individual disruption of REGNASE-1 and PTPN2, two top hits identified in our in vivo competitive***
187 ***assay, improved in vivo tumor control capacities of CAR-T cells***

188 To validate whether the selective advantage of top screening hits translated into improved tumor
189 control in vivo, we generated lentiviral vectors expressing gRNAs targeting *PTPN2* and *REGNASE-1*,
190 two of the most reproducible hits across donors and stress conditions. Despite a relatively
191 suboptimal gene editing efficiency, (Supplementary fig. 3 A), both *REGNASE-1* KO and *PTPN2* KO CAR-T
192 cells showed a clearly improved anti-tumor capacity. Compared to unmodified CAR-T cells, both
193 gene-KO strategies led to improved tumor control and extended survival (Fig. 4 A, B) demonstrating
194 the predictive value of our screening approach.

195 Mice were sacrificed at 28 days to allow comparison with the control condition. We confirmed a
196 markedly reduced tumor burden in the lungs of mice treated with *REGNASE-1* KO or *PTPN2* KO CAR-T
197 cells (Fig. 4 C). Then, we could observe a significantly higher number of *REGNASE-1* KO CAR-T cells at
198 the tumor site and circulating lymphoid organ, as assessed in the spleen (Fig. 4 D), whereas
199 surprisingly *PTPN2* KO had no notable effect on CAR-T cells numbers. These findings suggest distinct
200 mechanisms underlie the improved efficacy conferred by targeting the two genes. *REGNASE-1* KO
201 appears to systematically enhance *in vivo* CAR-T expansion, while *PTPN2* KO may provide a selective
202 advantage under stress conditions without promoting accumulation in in a more favourable context.

203 The greater number of *REGNASE-1* KO CAR-T cells in treated mice (Fig. 4 D) ensured an effective anti-
204 tumor response, yet it raises the question of potential toxicities.[67] To address this issue, we tested
205 in CAR-T cells combination of *REGNASE-1* KO (Supplementary fig. 3 B), with a safety switch system based
206 on inducible Caspase-9 (Fig. 4 E)[68], that has been successfully applied in clinics.[6] We observed that
207 modified CAR-T retain sensitivity to the iCas9 system (Fig. 4 F), proving these approaches could likely
208 assure safety of modified CAR-T cells therapies.

209

210 ***REGNASE-1 ablation enhances activation profile in tumor-infiltrating CAR-T cells***

211 To further characterise the effects of *REGNASE-1* and *PTPN2* knockout, we performed Cytometry by
212 Time of Flight (CyTOF) analysis on CAR-T cells isolated from the lungs (tumor site) of treated mice.
213 Uniform Manifold Approximation and Projection (UMAP) was used to summarise data from over 30
214 markers (Supplementary Tab. 1). Clustering patterns were consistent across samples from each
215 condition (Supplementary fig. 4 A), enabling to focus the analysis on three representative samples and to
216 confirm it in all replicates (Fig. 5 A, Supplementary fig. 4 A). UMAP identified four main clusters: CD4 T
217 cells, CD8 T cells, a minor CD4/CD8 double-positive group, and a very small CD4/CD8 double-negative
218 cluster. The main difference between conditions was a higher proportion of CD4+ cells in *PTPN2* KO
219 CAR-T cells, and more prominently in *REGNASE-1* KO CAR-T cells (Fig. 5 A, Supplementary fig. 4 A). Aside
220 from this, CTRL and *REGNASE-1* KO CAR-T cells more clearly differ, while *PTPN2* KO cells mostly
221 resemble to CTRL cells. (Fig. 5 A, Supplementary fig. 4 A)

222 The first difference in *REGNASE-1* KO CAR-T cells is the emergence of a distinct cluster within the CD4
223 population. This cluster is defined by co-expression of activation markers, HLA-DR, ICOS, CD28, and
224 immunomodulatory markers CTLA4 and PD1, all upregulated in *REGNASE-1* KO cells (Fig. 5 A, B,
225 Supplementary fig. 4B). Additionally, in these cells we could clearly detect expression of cytotoxic
226 molecules, with some, as granzyme A, showing broader and stronger expression than in other CD4

227 cells (Fig. 5D). These active, cytotoxic CD4+ cells represent a significantly large fraction of *REGNASE-1*
228 KO CAR-T cells, suggesting a key role in their enhanced expansion and tumor control.

229 Within the CD8 cluster, *REGNASE-1* KO cells showed a similar shift, with the emergence of a
230 resembling subpopulation (Fig. 5 C). These cells also show an increase in activation HLA-DR, ICOS,
231 CD28, and immunomodulatory markers CTLA4 and PD1 as their CD4 counterparts and maintained full
232 cytotoxic potential (Fig. 5 C, D). Although representing a smaller fraction of CD8 than CD4 cells, this
233 subset was consistently observed and significantly enriched in *REGNASE-1* KO CAR-T cells compared
234 to CTRL (Fig. 5 C, D, Supplementary fig. 4 C). Despite overall cell number expansion, CD8 T cells made up a
235 smaller proportion of total CAR-T cells in *REGNASE-1* KO samples, suggesting a stronger impact of this
236 modification on CD4 cells. Nonetheless these phenotypic data indicate a notable effect on CD8+ cells
237 as well.

238 Overall, KO of *REGNASE-1* appears to allow CAR-T cells to achieve and retain a stronger activation
239 upon tumor encounter, which could explain the large increase in CAR-T cells numbers, while
240 maintaining anti-tumor capacities, allowing for better tumor control and ultimately tumor clearance.

241

242 ***MED12 ablation, the lowest-scoring gene in our screening, increases in vitro proliferation and***
243 ***differentiation but reduces in vivo long-term efficacy in this model***

244 Unexpectedly, in our in vivo screen, knockout of at least three promising target genes was as
245 detrimental as inactivation of essential genes used as negative controls (RHOH, ZAP70, VAV1, LCP2).
246 MED12 was the lowest-scoring hit, leading us to test whether its loss could impair CAR-T tumor
247 control in our model. Tumor-bearing mice were treated with a high dose of CAR-T cells, either
248 unmodified or *MED12* KO (Supplementary fig. 5 A). At this dose, unmodified CAR-T cells efficiently
249 cleared tumors within 21 days, with only one mouse relapsing later. Initially, MED12 KO CAR-T cells
250 also reduced or eradicated tumors in some mice. However, tumors later reappeared, persisted, and
251 regrew, leading to death in most MED12 KO-treated mice (Fig. 6 A,B). These results suggest that,
252 under our conditions, *MED12* KO would not impair CAR-T functionality but compromises their long-
253 term persistence in mice.

254 To better understand this effect and relate it to prior findings on this genetic modification, we further
255 characterised *MED12* KO CAR-T cells. Firstly, we observed that in the screening, CAR-T cells receiving
256 MED12-targeting gRNAs showed enhanced expansion during production (Fig. 6 C), which we
257 confirmed in an independent experiment (Supplementary fig. 5 B). Although this early in vitro expansion
258 is outweighed by later in vivo depletion, it shows that this modification could be beneficial under
259 different conditions. Phenotypically, MED12 KO CAR-T cells showed greater differentiation,
260 consistent with previous reports [26], with a marked loss of stem cell memory T cells in both CD4 and
261 CD8 compartments (Fig. 6 D, Supplementary fig. 5). This accelerated differentiation may explain the initial
262 proliferation advantage, but also the reduced persistence *in vivo*, as previously shown in the field.
263 [69, 70]

264

265

266

267 ***A high selective pressure in vitro mimics in vivo screening results, despite attenuated effects***

268 We reasoned that for studying certain characteristics, an in vitro surrogate assay could be
269 informative as long as its results mirrored those from the *in vivo* model. Therefore, we established a
270 high selective pressure *in vitro* assay, restimulating CAR-T cells, by seeding them on irradiated A549
271 cells, every 5 days over 35 days (Fig. 7 A). Under these conditions, CAR-T cells initially expanded
272 strongly and eradicated tumor cells, followed by stagnation and a clear decline in cell numbers (Fig. 7
273 B). Analysis of gene-KO subpopulations variations, highlighted results similar to those in vivo: *SOCS1,*
274 *REGNASE-1, PTPN2* and *P16INK4A* KO remained top hits, though their advantage was less
275 pronounced. Likewise, genes with negative effects in vivo also scored lower here, though their
276 disadvantage was less consistent between donors (Fig. 7 C).

277

278 ***Effects of signaling differences on gene editing strategies efficacy in vitro***

279 After confirming the in vitro assay could sufficiently reproduce the *in vivo* results, we used it to
280 explore how signaling modifications influences gene editing efficacy. First, we asked whether
281 stimulation via the TCR versus the CAR would affect the impact of gene edits on T cell expansion. To
282 mimic TCR signaling, we used anti-CD3/anti-CD28-loaded polymers, while CAR signaling was
283 triggered by exposure to irradiated tumor cells. Notably, after 14 days, knockout of essential TCR
284 pathway genes had a stronger negative effect under TCR-like stimulation than CAR stimulation.
285 Conversely, KO of TCR pathway regulators showed a more beneficial effect in TCR-stimulated cells
286 (Fig. 7 D). Although CAR signaling is designed to mimic TCR engagement, they differ significantly [71,
287 72], and our findings highlight how such differences influence the efficacy of gene editing strategies,
288 raising a warning on translatability of data obtained from studies on T cells for CAR-T cells
289 amelioration.
290
291 We next asked whether these results could be explained by the different co-stimulation signal.
292 Notably, CD28 and 4-1BB co-stimulation is a one of the main differences across CAR-T products [73,
293 74]. We redesigned our CAR construct to include a CD28 domain instead of 4-1BB and tested these
294 CAR-T cells in the *in vitro* re-stimulation assay. CD28 CAR-T cells showed reduced persistence
295 compared to 4-1BB ones (Supplementary fig. 6 A), which forced to adapt our test, reducing re-
296 stimulation frequency to once every 7 to 10 days (Supplementary fig. 6 B). Under these conditions, gene
297 KO subpopulation changes were less pronounced, only partially reproducing earlier findings. *SOCS1*
298 and *PTPN2* remained top hits, while *REGNASE-1* and *P16INK4A* KOs showed no clear benefit (Fig. 7 E).
299 Most interestingly though, we observed no major differences in gene-KO subpopulations selected in
300 CD28 and 4-1BB CAR-T cells (Fig. 7 E). These results support previous findings [73, 75] that co-
301 stimulatory domains impact CAR-T persistence, while do not seem to impact effects of gene editing
302 strategies in improving this feature in our settings.
303

304 ***A subcutaneous tumor model to study gene editing efficacy on longer term, within different tumor***
305 ***structure and for metastasis control***

306 We sought to translate our screening assay to a subcutaneous A549 tumor model to assess how and
307 if factors like time and tumor architecture affect gene editing strategy efficacy. In this model, CAR-T
308 cells infiltrate tumors sufficiently, though less effectively than in the lung model. Also in this case we

309 found conditions for partial tumor control without full eradication (Fig. 8 A, B). Tumor mass inversely
310 correlated with CAR-T cell numbers, though less strongly than in the orthotopic model (Fig. 8 C). As
311 before, CAR-T cells from tumors showed increased differentiation and exhaustion markers, along
312 with impaired function in ex vivo assays (Supplementary fig. 7 A, B, C). Interestingly, we could observe
313 that subcutaneous A549 tumors developed lung metastases, which were effectively controlled and
314 cleared by CAR-T cell treatment (Fig. 8 D, E).

315

316 ***Ablation of SOCS1 is the most enriched target gene in the subcutaneous tumour model and for***
317 ***controlling metastases***

318 We repeated our screening in the subcutaneous model, treating mice with modified CAR-T cells and
319 sacrificing them 70–77 days later (Fig. 8 F). Sufficient CAR-T cell infiltration was detected in tumors
320 from 2 out of 3 T cell donors, with high variability in cell numbers (Supplementary fig. 7 D), nonetheless,
321 we could perform sequencing analysis on all these samples. As in the orthotopic model, we
322 confirmed top ranking of *SOCS1, PTPN2* and *P16INK4*, whereas for *REGNASE-1* KO we could observe a
323 positive effect, but not a consistent ranking across the two donors (Fig. 8 G). The most notable
324 difference was the significantly improved performance of *SOCS1* KO CAR-T cells, suggesting that this
325 genetic modification may offer a more sustained long-term advantage in a complex tumor
326 environment with limited infiltration (Fig. 8 G). Consistent with previous findings, *PRDM1* and *BATF*
327 KOs had a clear negative impact, while *MED12* KO effects were less defined in this context (Fig. 8 G).

328 We also analyzed the lungs, as we observed the development of lung metastases in this model,
329 detecting CAR-T cells at proportions similar to those in the orthotopic model (Supplementary fig. 7 E)
330 leading to control of the tumor mass (Fig. 8 H). Gene KO subpopulation enrichment analysis confirmed
331 *SOCS1* as the top scorer, followed by *PTPN2* and *REGNASE-1* (Fig. 8 I). These results were consistent
332 with findings in the subcutaneous tumor, making it difficult to distinguish whether selection effects
333 are a result of local proliferation or a consequence of CAR-T cell recirculation from the primary
334 lesion. Interestingly, for genes like *REGNASE-1* and *SOCS1*, the screening results appeared somewhat
335 intermediate between the orthotopic lung tumor (Fig. 3 D) and subcutaneous tumor models (Fig. 8 G).

336

337 ***Application of the screening assay for the improvement of CAR-T cells mitochondria metabolism,***
338 ***another relevant phenotype in our context***

339 Finally, we wondered if our library could be applied, in parallel to *in vivo* screenings, to study other
340 CAR-T cell characteristics specifically relevant in a given context, to integrate results from these
341 readouts. We previously found that enhanced mitochondrial respiration improves CAR-T cell
342 migration and tumor control in this model [76]. To investigate this, we set up a screening assay to
343 identify gene KO subpopulations enriched in cells with top 10% high levels of the standard
344 mitochondrial marker MitoTracker expression compared to the bottom 10% (Fig. 9 A, B). Cells in these
345 groups had corresponding differences in mitochondrial content, confirmed by mtDNA quantification
346 (Fig. 9 C). By this screening we identified *PRDM1* and *IRF2* as top-scoring genes in CAR-T cells from all
347 three donors (Fig. 9 D).

348 We then produced individual KO CAR-T cells (Supplementary fig. 8 A) and confirmed increased
349 MitoTracker staining for both *PRDM1* and *IRF2* KOs (Fig. 9 E). We also detected higher mtDNA levels in

350 *PRDM1* KO cells, while *IRF2* KO showed large variability in mtDNA quantification (Fig. 9 F).
351 Nonetheless, we assessed whether these KOs could enhance CAR-T cell respiratory capacity and
352 *PRDM1* KO cells showed a significant increase in respiration, whereas *IRF2* KO had no impact (Fig. 9 G).
353 Finally, we confirmed that the increased respiratory capacity of PRDM1 KO CAR-T cells led to
354 improved migratory capacity in our 3D motility test, while no difference there was no difference for
355 *IRF2* KO (Fig. 9 H).

356 These results support the versatility of our screening for broader studies on CAR-T cells, applying
357 other readouts than just persistence. On the other hand, they highlight the importance of crossing
358 results of these studies, as for persistence readouts *PRDM1* KO proved unsuitable.

359

360

361 **CONCLUSION**

362 The once unforeseeable successes of CAR-T cell therapy come with the need for further
363 improvements, aiming to achieve remission in all leukaemia and lymphoma patients and extend
364 treatment to solid malignancies[1]. The first limitation to tackle, in hematologic malignancies and
365 most importantly in solid cancers, would be the poor proliferation and/or persistence of CAR-T cells
366 in patients[2, 4, 31]. In this context, several groups have made valuable contributions, proposing
367 therapy improvements, with gene editing strategies holding great promise[9, 10].

368 Alongside discovering new strategies, it will be necessary to evaluate them in specific contexts.
369 Indeed CAR-T therapies widely differ in terms of the tumor and antigen targeted, the CAR construct
370 design, the production pipeline, and predicted patient profiles, all impacting their efficacy. [19-23]

371 Different whole genome CRISPR-KO approaches have been applied to study T or CAR-T cell
372 improvements, and key lessons can be drawn from them. First, that applying such approaches *in vivo*
373 requires ingenious strategies to overcome limitations intrinsic to these models [25, 27-29, 77].
374 Second, that context specific studies would be crucial, as results from these investigations do not, or
375 only partially confirm one another. [24-29, 77]

376 In this work, we propose a method for focused small-scale studies in pertinent models to identify
377 genetic modifications effective for a given CAR-T therapy. This approach allowed us to identify genes
378 *REGNASE-1, SOCS1, PTPN2*, and *P16INK4A* that gave CAR-T cell a long-term selective advantage in an
379 orthotopic tumor model. Later, we performed proof-of-concept validation of two out of these genes,
380 *REGNASE-1* and *PTPN2* confirming that their individual could enhance CAR-T cell antitumor efficacy.
381 Suggesting that genes identified by our screening would be prime targets for improving CAR-T
382 therapy in lung adenocarcinoma.

383 Surprisingly, we revealed that some genes, such as *MED12*, *PRDM1*, and *BATF*, led to negative
384 selection in our screening. While these results do not undermine the potential of these
385 modifications, given the convincing positive effects on CAR-T cells in the context of other studies, [11,
386 26, 54], they emphasize the need for context-specific analyses.

387 An approach like the one proposed can also provide insights into the underlying biological
388 mechanisms of CAR-T success or failure. For instance, we observed that *REGNASE-1* KO CAR-T cells
389 had a marked over-representation of highly activated, pre-exhausted, and cytotoxic CD4 and CD8

390 cells in the tumor site, correlating with antitumor efficacy in the orthotopic lung tumor model. This
391 increased activation could explain the improved proliferation of these cells, and does not seem to
392 compromise cytotoxic properties, ensuring antitumor efficacy. The upregulation of
393 immunomodulatory markers seems a consequence of high activation, not detrimental to these
394 qualities. These cells share characteristics of CD8 Tpex cells [78], associated with improved
395 persistence of CAR-T cells and better tumor control, reportedly enriched in *REGNASE-1* KO CAR-T
396 cells in mice [79].
397 Conversely, MED12 KO CAR-T cells showed accelerated differentiation during the production phase,
398 which may explain their early in vitro proliferation and potentially the improved efficacy in other
399 models [26], but proved deleterious in our orthotopic lung tumor model.
400
401 Another key aspect for CAR-T therapy development is the need to use diverse models and assays,
402 each addressing specific aspects of the treatment[80, 81]. Therefore, CAR-T cells improvement driven
403 by gene-modification strategies could benefit from integrating multiple readouts.
404
405 For CAR-T therapy in a given pathology, different *in vivo* models may be valuable. The orthotopic lung
406 tumor better mimics CAR-T trafficking in lung cancer and tumor growth in a more physiological niche.
407 [82] Conversely, subcutaneous models suit longer-term studies and better reflect structural barriers
408 hindering CAR-T therapy in solid tumors. [83, 84]
409 In this study on lung adenocarcinoma, we used both models and found that while *SOCS1* KO matched
410 *REGNASE-1* KO in the orthotopic model, it significantly outperformed it in the subcutaneous one.
411 While it is hard to predict which model would better reflect real life conditions in patients, combining
412 both readouts improves confidence in identifying *SOCS1* KO as a promising strategy for CAR-T
413 enhancement in lung adenocarcinoma.
414
415 One major promise of CAR-T therapy in solid tumors is widespread tumor eradication and enhanced
416 immunosurveillance, eliminating metastases along with primary lesions to ensure relapse-free
417 remission [85, 86].
418 In this study, we assessed CAR-T cell genetic modifications enriched in both primary tumor and
419 metastatic site within the same mice. We observed a general concordance of results, possibly due to
420 local selection of similar genes or CAR-T cell recirculation. Interestingly, for KO of *SOCS1* and
421 *REGNASE-1*, results in lung metastases were intermediate between those in the subcutaneous
422 tumors and the lungs in the orthotopic models. This may reflect niche-specific preferences for certain
423 gene editing strategies and further studies in this direction would be of great interest.
424
425 Further addressing the issue of context-specific readouts, various examples arise: in some settings,
426 PD-L1-induced inhibition may be the main obstacle, while in others it may be nutrient deprivation or
427 hypoxia within the tumor site [87-89]. Developing gene editing strategies to tackle these challenges
428 could be valuable as secondary readouts to *in vivo* persistence.
429
430 In our tumor model, we previously demonstrated the importance of strong mitochondrial
431 metabolism and CAR-T cell migration[76]. Using a screening based on high MitoTracker signal, we
432 identified *PRDM1* KO as enhancing mitochondrial mass, respiration, and migration. However, our
433 other screenings showed this modification impairs CAR-T cell expansion and persistence, making it
434 unsuitable for improvement in this context.

Results from different readouts may also guide more complex editing approaches, combining multiple gene KOs. It was shown that KO of *REGNASE-1, PTPN2*, and *SOCS1*, prioritized in our study, can be combined with additive effects[28]. Given current limitations of CAR-T therapy in lung tumors, such a 'radical' approach could be envisaged. In this work, we also demonstrate the efficacy of a suicide gene to eliminate both REGNASE-1-modified and non-modified CAR-T cells. This safety switch could be essential to support development of these highly effective CAR-T cells while ensuring toxicity control.

To conclude, we propose a new CRISPR-KO screening approach in CAR-T cells, tailored to improve specific therapies in relevant *in vivo* models. Notably, a recent study (preprint [90]) using a similar strategy in multiple myeloma also confirmed the importance of *REGNASE-1*, *SOCS1*, and *PTPN2*, while *MED12* inactivation showed neither a positive nor negative effect, despite inclusion in their gRNA library. These data suggest some gene KOs may have broad efficacy, even though we could observe quantitative differences of such effects in different models. Others may be highly context-dependent, ineffective or even harmful in some settings, but beneficial in others, highlighting the value of context-specific studies.

MATERIALS AND METHODS

Study approvals

All human studies complied with French biomedical research regulations and the principles of the 1975 Helsinki Declaration and its revisions. Peripheral blood samples from adult donors were obtained from the Etablissement Français du Sang (EFS) under agreement 18/EFS/030, with informed consent for research. Samples were anonymized.

NOD.Cg-Prkdc^(scid)Il2rg^(tm1Wjll)/SzJ (NSG) mice were purchased from The Jackson Laboratory (strain 005557) and housed under pathogen-free conditions at the Cochin Institute Animal Facility, in same-sex cages of 5–6 mice. Environmental parameters were regulated per FELASA guidelines, with cage enrichment provided. Health monitoring and pathogen screening were routinely conducted. Animal discomfort was minimized, and usage was reduced in line with Directive 86/609/EEC. Both sexes were used, with balanced distribution among experimental groups, and euthanasia was performed by cervical dislocation. The protocol was approved by Paris Descartes University (CEEA 17-039) and the French Ministry of Research (APAFiS 15076 and 49768).

Cell Culture and Reagents

Peripheral blood mononuclear cells (PBMCs) were isolated via Ficoll gradient centrifugation (800 g for 20 min, RT) and cryopreserved in 90% fetal bovine serum (FBS) (Thermo Fisher, A3840002) and 10% DMSO (Thermo Fisher, 327182500). For CAR-T cell production, PBMCs were cultured in RPMI 1640 medium (Thermo Fisher, 21875) with 10% FBS, 2 mM L-glutamine (Thermo Fisher, 25030081), and 100 U/ml penicillin/streptomycin (Thermo Fisher, 15140130), supplemented with 25 ng/ml IL-7 (Miltenyi, 130-095-363) and IL-15 (Miltenyi, 130-095-765). Cells were activated 24 hours post-thaw with T cell TransAct (Miltenyi, 130-111-160) at a 1:200 dilution for 48 to 96 hours.

For experiments with the sgRNA-expressing lentiviral library or the iCasp9-expressing virus, 1 ug/ml puromycin (Thermo Fisher, A11138-03) was added two days post-nucleofection for three days, then reduced to 0.5 µg/ml until the end of CAR-T cells production. Human A549 (mCherry^{+}, Luciferase^{+})

479 and HEK-293T tumor cells were cultured in DMEM medium (Thermo Fisher, 11995) with 10% FBS, 2
480 mM L-glutamine and 100 U/ml penicillin/streptomycin. All cell lines were tested for mycoplasma
481 contamination.
482
483 ***T cells viral transduction and gene editing***
484 For experiments with the sgRNA-expressing lentiviral library or individual sgRNA-expressing viruses,
485 cells were activated, then infected at 24h with 2.5 µl/ml of lentiviral pool or individual sgRNA
486 lentiviruses. At 48h, the medium was changed, and cells were infected with 100 µl/ml of CAR-
487 expressing viruses and lentiBOOST (Revvity, SB-A-LF-901-01) at 1:200. At 72h cells were washed,
488 divided into 5×10^5 aliquots, resuspended in 16.4 µl P3 and 3.6 µl Supplement Reaction solutions
489 from P3 Primary Cell 4D X Kit S (Lonza, V4XP-3032), and 5 µg of Cas9 protein (Thermo Fisher,
490 A36497). Electroporation was performed using the Amaxa 4D Nucleofector (Lonza), following the
491 manufacturer's instructions. After 30 minutes of recovery at 37°C, cells were cultured for 24 more
492 hours under stimulation conditions. For procedures without gene editing, only CAR virus infection
493 was performed. In the suicide gene experiment, cells were infected at 24h with 100 µl/ml of iCASP9-
494 expressing viruses, at 48h with CAR-expressing viruses, and at 72h sgRNAs (Thermo Fisher, A35534)
495 were added in a 3:1 molar ratio to Cas9 protein during nucleofection. The REGNASE-1 sgRNA used for
496 RNP editing had target sequences 5'-AAGGAGGTCTTCTCCTGCCG-3' and 5'-
497 CAGTGTTTGTHCCATCCTGG-3'.[67]
498
499 ***Lentiviruses design and production***
500 To generate anti-EGFR 4-1BB-CAR, scFv sequences from nimotuzumab Ab (IMGT/2Dstructure-DB INN
501 8545H, 8545L) were introduced into the expression cassette encoding CD8 hinge and
502 transmembrane domains (194–248 Aa, GenBank: AAH25715.1), 4-1BB costimulatory domain (214–
503 255 Aa, GenBank: AAX42660.1), CD3z signaling domain (52–163 Aa, GenBank: NP_000725.1), and
504 GFP coding sequence (downstream of IRES).
505 To generate anti-EGFR CD28-CAR, 4-1BB was replaced with CD28 (GenBank: NM_001243078.2) in an
506 identical new vector (Vector Builder VB240303-1098rav).
507 Lentivirus expressing FK506-binding protein 12 (F36V) fused with human CASPASE-9 protein (1-134
508 AA deleted) and linked to HA tag was purchased as commercially available (Vector Builder VB900176-
509 7377zdg).
510 Lentiviral bank expressing gRNAs (Vector Builder Lib230420-1523hhp) was custom designed by
511 Vector Builder, targeting 50 genes of interest and 4 essential genes in T-cell activation (LCP2, RHOH,
512 VAV1, ZAP70). For each gene, 4 gRNAs were designed, including 2 previously described in the
513 literature when available. 20 non-targeting gRNAs were also included as controls.
514 Custom sgRNA expressing plasmids were designed on demand, including sgRNA targeting *EGFP*
515 (Vector Builder VB230314-1357xnw, sequence: 5'-GGGCGAGGAGCTGTTCACCG-3'), *RINF* (Vector
516 Builder VB230314-1123mnq, sequence: 5'-GTTGCTTTTGTCCACCGCCA-3'), scramble (Vector Builder
517 VB240125-1049dfy, sequence: 5'-ACGTGGGGACATATACGTGT-3'), *REGNASE*-1 (Vector Builder
518 VB240125-1038zad, sequence: 5'-TTCACACCATCACGACGCGT-3'), *PTPN2* (Vector Builder VB240216-
519 1035aey, sequence: 5'-AGTGCAGGCATTGGGCGCTC-3'), *MED12* (Vector Builder VB240715-1614nfg,
520 sequence: 5'-TAACCAGCCTGCTGTCTCTG-3'), *PRDM1* (Vector Builder VB240918-1470wdv, sequence:
521 5'-TCGATGACTTTAGAAGACGT-3'), and *IRF2* (Vector Builder VB240918-1473bwg, sequence: 5'-
522 GGATGCATGCGGCTAGACAT-3').
523

524 Lentiviral particles were produced by transient co-transfection (polyethylenimine:DNA at 3.5:1 ratio)
525 of HEK 293T cells with the plasmids expressing the sequence of interest and second-generation
526 packaging plasmids psPAX2 and pMD2.G (Addgene, 12260 and 12259). Viral supernatants were
527 collected at 48 and 72 h post-transfection, concentrated by ultracentrifugation at 25,000 g for 2 h,
528 and stored at −80 °C.
529
530 ***Gene editing assessment by deconvolution assays***
531 DNA extraction from bulk-edited and control CAR-T cells was performed using the FastPure
532 Blood/Cell/Tissue/Bacteria DNA Isolation Mini Kit (Vazyme DC112-01-AB). Cells were lysed with
533 proteinase-K (Vazyme, DE102-01) at 56°C, and DNA was isolated using silica gel column purification.
534 Gene editing efficiency was assessed by PCR amplifying the genomic region surrounding the CRISPR-
535 Cas9 sgRNA target site; then PCR amplicons were then subjected to Sanger sequencing (Eurofins
536 tubeSeq supreme service). Sequencing data were analyzed using DECODR (ChristianaCare) [91] via
537 the Latch.bio online console. DECODR uses a deconvolution algorithm to interpret mixed sanger
538 sequencing chromatograms, quantifying indel frequencies.
539
540 ***Orthotopic and subcutaneous tumor models***
541 For the orthotopic tumor model, 4 × 10^6 human A549 cells (mCherry+ Luciferase+) were injected
542 intravenously (i.v.) into the tail vein of 6 to 10 weeks-old NSG nude mice (balanced sex distribution
543 across conditions) in most experiments. In a screening experiment, 20 x 10^6 A549 cells were
544 injected instead.
545 For tumor growth follow-up, 3 days after i.v. injection of A549 cells, mice were injected i.v. with anti-
546 EGFR CAR T cells (number specified in the text). Tumor growth in the lungs was monitored by
547 bioluminescence using the PhotonIMAGER system (Biospacelab) and M3Vision software
548 (Biospacelab, version 1.2.1.32016). Tumor burden was evaluated using a grid based on
549 bioluminescence, behaviour, appearance, weight, etc., with mice sacrificed upon reaching the
550 endpoint threshold score.
551 For the subcutaneous tumor model, 5 × 10^6 A549 cells were injected subcutaneously (s.c.) into the
552 right flank of 2-month-old NSG nude mice (balanced sex distribution). For infiltration analysis, after
553 5/6 weeks, mice were injected i.v. with 5 × 10^6 anti-EGFR CAR T cells and sacrificed 4 days later for
554 the same analyses as the orthotopic model. For tumor growth follow up, 14 days post-injection, A549
555 tumor-bearing mice were i.v. inoculated with 7 × 10^6 anti-EGFR CAR T cells or 5 × 10^6 CAR T cells
556 modified with the lentiviral bank, and tumor growth was followed by caliper measurement for 9-11
557 weeks. An evaluation grid was also used for this model, adapted for subcutaneous tumor mass
558 measurement, with mice sacrificed upon reaching the endpoint score.
559
560 ***Infiltration analysis***
561 For tumor infiltration assessment 3 weeks after tumour injection (4 × 10^6 human A549 cells
562 (mCherry+ Luciferase+)), mice were infused i.v. with 5 × 10^6 anti-EGFR CAR T cells, and after 4 days,
563 they were sacrificed and lungs collected.
564 Lung or subcutaneous tumor samples were fixed overnight (o.n.) with PLP solution (1%
565 paraformaldehyde, 2 mM lysine-HCl, 550 mg/L NaIO4) at 4 °C, cut into 1–2 mm^3 pieces, embedded in
566 7% agarose (Sigma Aldrich A0701), and sectioned into 150 µm-thick slices using a vibratome (VT
567 1000 S, Leica). For extracellular staining, slices were incubated for 1 h at RT with 0.5% BSA in DPBS.
568 The slices were placed onto Millicell 0.4 µm organotypic inserts (Millipore PICMORG50), and 30 µl of

569 0.5% BSA/DPBS with the desired Abs were added. A metal ring kept the solution in place, and Abs
570 were incubated o.n. at 4 °C. The following day, slices were washed twice in DPBS and mounted on
571 Superfrost microscope slides (Epredia J1800AMNZ) using Vectashield antifade mounting medium
572 (VectorLabs H-1900). The following antibodies were used (200 ng/slice): FITC-anti-CD3 (Biolegend
573 344804, clone SK7) and PE-anti-EpCAM (Biolegend 324206, clone 9C4). 4',6-Diamidino-2-
574 phenylindole (1/1000) was used to stain nuclei. Images were captured with a spinning-disk
575 (Yokogawa CSU-W1 T1) Ixplore IX83 microscope (Olympus) equipped with an ORCA-Flash 4.0 V3
576 (sCMOS Hamamatsu) camera and CellSens Dimension software (Olympus, v4.1.1). CAR-T cells
577 infiltration was analyzed using an ImageJ threshold mask to identify EpCAM+ areas (tumor islets) and
578 CD3+ areas (T cells). "Subtract" or "multiply" ImageJ commands were used to define T cells in tumor
579 stroma or islets, respectively. Raw data from these infiltration experiments were previously
580 employed as control condition in figure 7 B and E of another publication from our group [76], Data
581 have been here used for a different analysis to study and compare CAR-T cells infiltration within the
582 tumour tissue in the two models.
583
584 ***HES staining on tissue samples and machine learning metastatic burden quantification***
585 Tissues were fixed in 4% PFA for 24 hours, dehydrated in graded ethanol, isopropanol, and xylene
586 (Thermo Fisher, A11358.0F), then embedded in paraffin for FFPE storage. Sections were cut into 6
587 slices (4 µm thick, 150 µm apart), using a microtome (Autosection, Sakura). Slides were stained on
588 the SPECTRA stainer (Leica) with H&E, deparaffinized, rehydrated, rinsed, incubated in Mayer's
589 haematoxylin for 3 minutes, rinsed, stained in erythrosine for 5 minutes, followed by 5 minutes in 1%
590 alcoholic saffron. Digitalized Images were obtained Stained slides were scanned at 20x magnification
591 using the Lamina Slide Scanner (Perkin Elmer) and analyzed with Case Viewer software (v 2.2).
592
593 From these images, 4 cropped areas (4.5x magnifications) from at least 2 different slices were
594 analyzed with InForm® software. Cropped images were converted to optical density with eosin and
595 purple haematoxylin channels. Tissue segmentation was performed by categorizing regions as no
596 tissue, healthy tissue, and tumor tissue. At least 10 areas per category were used to train the
597 machine learning algorithm. Segmentation was then automated and visually inspected, with
598 corrections made manually. The percentage of metastatic area was calculated as the ratio of
599 metastatic area to the sum of healthy and tumor tissue areas.
600
601 ***Tumors and organs dissociation***
602 Tumor-bearing mice lungs were cut into 1-2 mm pieces, digested with Liberase (Roche 5401119001)
603 at 37 °C for 30 minutes, then smashed using a 70 µm Cell Strainer filter (Corning 352350). Collected
604 cells were stained for flow cytometry (BD Fortessa) or pelleted for DNA extraction. Subcutaneous
605 tumors were processed similarly to obtain single-cell suspensions, stained or pelleted for DNA
606 extraction. Spleens were collected, smashed using a 70 µm filter, and cells were processed as above.
607
608 ***Tumor infiltrating CAR-T cells isolation***
609 CAR-T cells were isolated from single-cell suspensions using the human CD45 MicroBead Kit
610 (Miltenyi, 130-121-563) and LS Columns (Miltenyi, 130-042-401). Cells were resuspended in MACS
611 buffer, incubated with CD45.1 MicroBeads at 4°C for 15 minutes applied to LS Columns, washed, and
612 eluted with buffer. Collected CAR-T cells were either stained for flow cytometry (BD Fortessa) for the

613 lung tumor characterisation experiment or cultured for 48 hours and used in cytotoxicity and
614 proliferation assays for both lung and subcutaneous tumor experiments.
615
616
617
618 ***Cytotoxicity assays***
619 Cytotoxic activity of in vitro expanded and tumor-extracted anti-EGFR 4-1BB-CAR T cells was assessed
620 using mCherry-expressing A549 cells. A549 cells were seeded at 20×10^5 cells per 250 µl in 96-well
621 plates (Corning 351172) with DMEM. After 48 hours (time 0 h), plates were irradiated with 50 Gy
622 using a BIOBEAM GM 2000 (Ekert and Ziegler). anti-EGFR 4-1BB-CAR T cells were added at a
623 CAR:target ratio of 4:1 in RPMI medium, without cytokines. In the experiment involving CAR-T cells
624 extracted from subcutaneous tumors, ratios of 1:2 were used, because of the low number of CAR-T
625 cells recovered. A549 cell viability was determined by measuring the mCherry-positive area at
626 different time points: A fluorescence microscope was used in the experiment shown in Figure 2, and
627 an Incucyte S3 (Sartorius) was used for all others. The mCherry-positive area was compared between
628 wells with and without CAR T cells.
629
630 ***In vitro proliferation assays***
631 In vitro cultured and tumor-isolated anti-EGFR 4-1BB-CAR T cell proliferation was evaluated by trypan
632 blue corrected living cell counting. Cells were cultured for 48 hours in complete medium, then
633 stimulated with anti-CD3/CD28 conjugated TransAct (Miltenyi, 130-111-160) at 1:200 for 48 hours.
634 Proliferation was followed for 7 days after activation.
635
636 ***Flow cytometry***
637 FSC-A/SSC-A gating and LIVE/DEAD™ Fixable Blue Dead Cell Stain Kit (Invitrogen, L23105) were used
638 to define live and dead cells. Extracellular proteins were stained with antibodies (1:100 dilution):
639 BV785 CD45 (Biolegend, 304048), PE CD45 (Biolegend, 368509), BV650 CD4 (Biolegend, 317436),
640 BUV737 CD8 (BD Biosciences, 612754), BV711 CD45RA (Biolegend, 304138), APC CD45RO (Biolegend,
641 304210), APC-Cy7 CD27 (Biolegend, 302816), PE-Cy7 CCR7 (Biolegend, 353225), APC PD-1 (Miltenyi,
642 REA1165), BV421 TIM3 (Biolegend, 345007), BV786 LAG3 (Biolegend, 369321). T cell subpopulations
643 were defined as follows: stem cell memory-like (Tscm, CD45ROnegCCR7pos or CD45RAposCD27pos),
644 effector-like (Teff, CD45ROnegCCR7neg or CD45RAposCD27neg), central memory-like (Tcm,
645 CD45ROposCCR7pos or CD45RAnegCD27pos), effector memory-like (Tem, CD45ROposCCR7neg or
646 CD45RAnegCD27neg). For Anti-EGFR 4-1BB-CAR or sgRNA expression, respective reporter genes
647 EGFP and mCherry fluorescence signals were analyzed. Mitochondrial mass was assessed by
648 incubating cells with 10 nM MitoTracker Deep Red (Thermo Fisher M22426) for 20/30 min at 37 °C,
649 followed by washing and analysis. All analyses were performed with a BD Fortessa (FACSDiva
650 software v6.1.3).
651
652 ***Correlation study on bioluminescence and infiltrating CAR-T cells % data***
653 At the experiment endpoint, tumor charge assessed by bioluminescence and CAR-T cell abundance
654 determined by flow cytometry were analyzed for correlation. Tumor charge confidence intervals for
655 each point were used for goodness-of-fit assessment, defined by the standard deviation of photon
656 rates (oscillating during measurement). After testing simple models, the best fit, evaluated by log-
657 likelihood maximization, was a power law:

658 $\boldsymbol{Y = A * X^B}$, with $\boldsymbol{A = 4.8 * 10^6}$ and $= \boldsymbol{-8.6 * 10^{-1}}$
659 Optimization assumed Gaussian-like noise to avoid penalizing data-points with large error bars. This
660 convention is widely used in counting experiments and justified in the literature [92]. No systematic
661 error in measurements was considered.
662
663 ***SgRNA readout by deep sequencing***
664 The sgRNA library readout was performed using PCR amplicon sequencing. Genomic DNA was PCR
665 amplified with adapters P5 and P7 bound custom primers (Eurofins) targeting a 350 bp vector region
666 containing the sgRNA cassette, using adapters P5 and P7.
667 Adapter-Forward: ACACTCTTTCCCTACACGACGCTCTTCCGATCT-TTGCATATACGATACAAGGCTGT
668 Adapter-Reverse: GACTGGAGTTCAGACGTGTGCTCTTCCGATCT-ACAAAGTTGGAATTCGGTACCTC
669 PCR was carried out with Platinum™ SuperFi II Master Mix (ThermoFisher, 12368010) and 5% DMSO,
670 with the following cycling conditions: 98°C for 8 minutes, 35 cycles of (98°C for 30 s, 58°C for 30 s,
671 72°C for 1 min), and 72°C for 10 minutes. Each reaction used 2 µg gDNA, with 3 independent
672 reactions per sample. PCR products were pooled, gel-purified with a 2% agarose gel and FastPure Gel
673 DNA Extraction Kit (Vazyme DC301-01), then normalized. The samples were sequenced by Eurofins
674 Genomics using the NGSelect Amplicon Illumina MiSeq service, producing 60K reads per sample with
675 basic quality control trimming of FASTQ files.
676
677 ***MAGeCK analysis of gene KO subpopulations enrichment***
678 For MAGeCK analysis, FASTQ files were processed with the MAGeCK -count algorithm to generate
679 count tables, which were then input into the MAGeCK -test algorithm.
680 (https://sourceforge.net/p/MAGeCK/wiki/Home/) The "mean" setting was used for LFC calculation,
681 and normalization was set to "total" with non-targeting control sgRNAs for RRA null distribution,
682 except for of subcutaneous tumor and lung samples from this experiment, where all gRNAs were
683 used for normalization due to the extremality of data in these settings, allowing a more conservative
684 but more effective calculation of p-values. LFC data were corrected to the mean LFC of non-targeting
685 gRNAs, and ranking was done with MAGeCK RRA for most analyses. In the case of subcutaneous
686 tumor and lung samples from this experiment, LFC-based ranking was applied, again to correct for
687 the extremality of data. P-values and FDR values indicated for screening experiments are reported as
688 calculated by the MAGeCK algorithm.
689
690 ***Inducible cell death experiment***
691 iCASP9-expressing CAR-T cells were stimulated with anti-CD3/CD28 TransAct (Miltenyi, 130-111-160)
692 at 1:200 concentration for 48 hours. Cells were reseeded at $1x10^6$ cells/ml and treated with 5 nM
693 AP20187 (MedChemExpress HY-13992) or vehicle DMSO solution, in fresh medium. Cell survival was
694 assessed at different time points by Fixable Live/Dead Blue (Thermofisher, L23105) staining,
695 correcting for the actual number of cells when reductions were observed compared to time 0.
696
697 ***CyTOF staining and data analysis***
698 Frozen samples were thawed, washed in PBS with 0.5% BSA (BSA; Sigma-Aldrich, A7030), 0.02%
699 sodium azide, and 15 µg/mL DNase, and stained with a surface antibody cocktail in PBS containing
700 0.5% BSA and 0.02% sodium azide for 15 minutes at RT (see Supplementary Table X for antibody
701 details). Viability was assessed by incubating with 5 µM cisplatin for 5 minutes. After 2 washing steps,
702 cells were permeabilized with Cyto-Fast Fix/Perm Solution (BioLegend) for 30 minutes at RT, stained

703 intracellularly with anti-Perforin, anti-Granzyme A, anti-Granzyme B, anti-Granzyme K, and anti-CTLA-
704 4 antibodies for 30 minutes at RT in permeabilization buffer, and fixed in 2% PFA overnight. DNA was
705 stained as described previously. [93] Antibodies were obtained from suppliers listed in
706 Supplementary Table 1 and conjugated following Standard Biotools' protocol. CyTOF acquisition was
707 conducted as previously described [94], and zero values were randomized using a custom R script,
708 consistent with previous CyTOF software defaults. UMAP analysis was performed using custom R
709 scripts with the "flowCore" and "uwot" packages as previously described, [95] and data
710 transformation applied with the "logicleTransform" function from "flowCore" (parameters: w = 0.25,
711 t = 16,409, m = 4.5, a = 0). For heatmap visualization, median intensity values were transformed
712 using a logical data scale, following the approach described by Moore and Parks[96]. A four-color
713 scale was used: black–blue (low), green–yellow (intermediate), and red (high) expression values
714
715 ***In vitro* restimulation assays**
716 For in vitro screening restimulation assays, 5×10^5 mCherry+Luciferase+ A549 cells were seeded in
717 12-well plates (Corning, 351143). After 24 hours, plates were irradiated with 50 Gy using a BIOBEAM
718 GM 2000 (Ekert and Ziegler), the medium was changed to Human T cell medium without interleukins,
719 and lentiviral-modified CAR-T cells were added at a 2:1 effector-to-target ratio, 3 biological replicates
720 were maintained for each donor in each condition. In the heavy restimulation assay, cocultures were
721 refreshed every 5 days with medium changes every 3-5 days for 35 days. In the mild restimulation
722 assay, cocultures were renewed every 10 days for 35 days. In both experiments cocultures were
723 downsized to smaller wells when needed due to CAR-T cells population contraction, maintaining
724 corresponding cells density. For the 14-day proliferation assay, CAR-T cells were cultured without
725 tumor cells and restimulated every 5 days with anti-CD3/CD28 TransAct (Miltenyi 130-111-160) for
726 48 hours. After 14 days, cells were harvested for DNA extraction and compared to cells from the
727 heavy restimulation assay at 14 days.
728
729 ***Flow Cytometric Sorting of High and Low MitoTracker Red-Expressing Cells***
730 For sorting based on mitochondrial mass, cells were incubated with 10 nM MitoTracker Deep Red
731 (Thermo Fisher M22426) at 37°C for 20-30 minutes, then washed and resuspended in sorting buffer
732 (PBS with 2% FBS and 1 mM EDTA). Cell sorting was performed on a BD FACSAria™ III, adjusting FSC
733 and SSC to exclude debris and doublets. Cells were gated by fluorescence intensity, and the highest
734 (MitoTracker-High) and lowest (MitoTracker-Low) 10% populations were sorted into RPMI-1640 with
735 20% FBS. Sorted cells were pelleted, frozen, and used for DNA extraction to analyse gene-KO
736 subpopulation frequency and mtDNA quantification.
737
738 ***mtDNA quantification by qRT-PCR***
739 Genomic DNA was extracted using the FastPure DNA Isolation Kit (Vazyme, DC112-01) and purified
740 with silica columns. qRT-PCR was performed on a LightCycler® 480 system (Roche) with the SYBR
741 Green I Master kit (Roche, 04707516001), with three replicates per sample. Analysis was performed
742 with LightCycler® 480 Software (version 1.5.1.62) Primers used: ND1-Fw 5'-
743 CCCTACTTCTAACCTCCCTGTTCTTAT-3', ND1-Rv 5'-CATAGGAGGTGTATGAGTTGGTCGTA-3', ND5-Fw 5'-
744 ATTTTATTTCTCCAACATACTCGGATT-3', ND5-Rv 5'-GGGCAGGTTTTGGCTCGTA-3', 18S-Fw 5'-
745 AGTCGGAGGTTCGAAGACGAT-3', 18S-Rv 5'-GCGGGTCATGGGAATAACG-3'. Mitochondrial DNA levels
746 were calculated using the ΔΔCt method with 18S rRNA as the reference gene.
747

In vitro motility assay with collagen gel and Analysis of T cell motility

T cells were stained with 100 nM Calcein Green (Invitrogen C34852) or Calcein Red Orange (Invitrogen C34851) for 20 min at 37 °C in DPBS, washed, and resuspended in 50 µl motility medium at 20×10^6 cells/ml. T cells were mixed with 100 ul of 2 mg/ml collagen solution (PureCol Bovine Collagen, CellSystem 5005), loaded into ibiTreat µ-Slide VI 0.4 (Ibidi 80606), and incubated at 37 °C for 1 h for collagen polymerization. T cell motility was recorded using a Nikon epifluorescence microscope, equipped with 37 °C heated-chamber, with ORCA-Flash 4.0 camera (C11440 Hamamatsu) and Metamorph software (version 7.10.2.240). Images (15 per condition, 30 s interval, 4/5 z-planes, z-distance of 15 µm) at 3 different stages were acquired using a 20x objective (binning rate 2). In most cases, T cells from two donors were stained with Calcein Green and Red, mixed, and added to collagen.

Motility analysis was done using TrackMate78 (ImageJ plugin, v.7.11.1) in 3D, LoG detector was used to identify spots (quality and maximal intensity filters applied) and Simple LAP Tracker to identify tracks (linking max distance 20 µm, closing-gap max distance 20 µm, frame gap 3) Only tracks with 10+ spots were analyzed. Motility Score was calculated as (% cells moving >10 µm) * (mean speed [µm/min] of moving cells). Analysis used original 3D images, considering z-axis displacement.

High-resolution respirometry with Oroboros device

The oxygen consumption rate (OCR) was measured using a 2 mL Oxygraph-2k respirometer (Oroboros). The electrode was calibrated at 37 °C, 100% and 0% oxygen, then CD8+ T cells (2 mL at 2.5×10^6 cells/mL) were added to the chamber. O2 consumption flux was measured in pmol/s. Oligomycin (0.5 µg/mL) was added to block complex V, followed by increasing concentrations of carbonyl cyanide m-chlorophenyl hydrazone (CCCP) to assess maximum respiratory capacity. Potassium cyanide (KCN) was added to measure non-mitochondrial respiration.

Statistical analysis

Data are shown as mean ± SEM or box-and-whisker plots. Statistical comparisons for normally distributed groups were performed using paired or unpaired two-tailed Student's t-test (for two-group comparisons) or One-way/Two-way ANOVA. For non-normally distributed data, the Wilcoxon Signed Rank Test (paired) or ANOVA on Ranks was used. Post hoc tests were applied for pairwise comparisons. Analyses were conducted using GraphPad (v8).

Graphics

All schematic representations were designed with Biorender.com

REFERENCES

1. Cappell, K.M. and J.N. Kochenderfer, *Long-term outcomes following CAR T cell therapy: what we know so far*. Nat Rev Clin Oncol, 2023. **20**(6): p. 359-371.
2. Fraietta, J.A., et al., *Determinants of response and resistance to CD19 chimeric antigen receptor (CAR) T cell therapy of chronic lymphocytic leukemia*. Nature Medicine, 2018. **24**(5): p. 563-571.
3. O'Rourke, D.M., et al., *A single dose of peripherally infused EGFRvIII-directed CAR T cells mediates antigen loss and induces adaptive resistance in patients with recurrent glioblastoma*. Sci Transl Med, 2017. **9**(399).

4. Albelda, S.M., *CAR T cell therapy for patients with solid tumours: key lessons to learn and unlearn*. Nat Rev Clin Oncol, 2024. **21**(1): p. 47-66.
5. Louis, C.U., et al., *Antitumor activity and long-term fate of chimeric antigen receptor-positive T cells in patients with neuroblastoma*. Blood, 2011. **118**(23): p. 6050-6.
6. Del Bufalo, F., et al., *GD2-CART01 for Relapsed or Refractory High-Risk Neuroblastoma*. N Engl J Med, 2023. **388**(14): p. 1284-1295.
7. Brown, C.E., et al., *Locoregional delivery of IL-13Rα2-targeting CAR-T cells in recurrent high-grade glioma: a phase 1 trial*. Nature Medicine, 2024. **30**(4): p. 1001-1012.
8. Sterner, R.C. and R.M. Sterner, *CAR-T cell therapy: current limitations and potential strategies*. Blood Cancer J, 2021. **11**(4): p. 69.
9. Tian, Y., et al., *Gene modification strategies for next-generation CAR T cells against solid cancers*. J Hematol Oncol, 2020. **13**(1): p. 54.
10. Dimitri, A., F. Herbst, and J.A. Fraietta, *Engineering the next-generation of CAR T-cells with CRISPR-Cas9 gene editing*. Molecular Cancer, 2022. **21**(1).
11. Zhang, X., et al., *Depletion of BATF in CAR-T cells enhances antitumor activity by inducing resistance against exhaustion and formation of central memory cells*. Cancer Cell, 2022. **40**(11): p. 1407-1422 e7.
12. Zou, Y., et al., *IKZF3 deficiency potentiates chimeric antigen receptor T cells targeting solid tumors*. Cancer Letters, 2022. **524**: p. 121-130.
13. Prinzing, B., et al., *Deleting DNMT3A in CAR T cells prevents exhaustion and enhances antitumor activity*. Science Translational Medicine, 2021. **13**(620).
14. Fraietta, J.A., et al., *Disruption of TET2 promotes the therapeutic efficacy of CD19-targeted T cells*. Nature, 2018. **558**(7709): p. 307-312.
15. Sutra Del Galy, A., et al., *In vivo genome-wide CRISPR screens identify SOCS1 as intrinsic checkpoint of CD4 + TH 1 cell response*. Science Immunology, 2021. **6**(66).
16. Jung, I.Y., et al., *CRISPR/Cas9-Mediated Knockout of DGK Improves Antitumor Activities of Human T Cells*. Cancer Res, 2018. **78**(16): p. 4692-4703.
17. Jafarzadeh, L., et al., *Targeted knockdown of Tim3 by short hairpin RNAs improves the function of anti-mesothelin CAR T cells*. Molecular Immunology, 2021. **139**: p. 1-9.
18. Rupp, L.J., et al., *CRISPR/Cas9-mediated PD-1 disruption enhances anti-tumor efficacy of human chimeric antigen receptor T cells*. Sci Rep, 2017. **7**(1): p. 737.
19. Mao, R., W. Kong, and Y. He, *The affinity of antigen-binding domain on the antitumor efficacy of CAR T cells: Moderate is better*. Frontiers in Immunology, 2022. **13**.
20. Weinkove, R., et al., *Selecting costimulatory domains for chimeric antigen receptors: functional and clinical considerations*. Clinical & Translational Immunology, 2019. **8**(5): p. e1049.
21. Wei, J., et al., *Target selection for CAR-T therapy*. Journal of Hematology & Oncology, 2019. **12**(1).
22. Watanabe, N., F. Mo, and M.K. McKenna, *Impact of Manufacturing Procedures on CAR T Cell Functionality*. Frontiers in Immunology, 2022. **13**.
23. Jaeger-Ruckstuhl, C.A., et al., *Phase I Study of ROR1-Specific CAR-T Cells in Advanced Hematopoietic and Epithelial Malignancies*. Clinical Cancer Research, 2025. **31**(3): p. 503-514.
24. Shifrut, E., et al., *Genome-wide CRISPR Screens in Primary Human T Cells Reveal Key Regulators of Immune Function*. Cell, 2018. **175**(7): p. 1958-1971.e15.
25. Dong, M.B., et al., *Systematic Immunotherapy Target Discovery Using Genome-Scale In Vivo CRISPR Screens in CD8 T Cells*. Cell, 2019. **178**(5): p. 1189-1204.e23.
26. Freitas, K.A., et al., *Enhanced T cell effector activity by targeting the Mediator kinase module*. Science, 2022. **378**(6620): p. eabn5647.
27. Zhao, H., et al., *Genome-wide fitness gene identification reveals Roquin as a potent suppressor of CD8 T cell expansion and anti-tumor immunity*. Cell Reports, 2021. **37**(10): p. 110083.

28. Wei, J., et al., *Targeting REGNASE-1 programs long-lived effector T cells for cancer therapy*. Nature, 2019. **576**(7787): p. 471-476.
29. Chen, Z., et al., *In vivo CD8+ T cell CRISPR screening reveals control by Fli1 in infection and cancer*. Cell, 2021. **184**(5): p. 1262-1280.e22.
30. Belk, J.A., et al., *Genome-wide CRISPR screens of T cell exhaustion identify chromatin remodeling factors that limit T cell persistence*. Cancer Cell, 2022. **40**(7): p. 768-786 e7.
31. Marofi, F., et al., *CAR T cells in solid tumors: challenges and opportunities*. Stem Cell Research & Therapy, 2021. **12**(1).
32. Qu, J., et al., *Chimeric antigen receptor (CAR)-T-cell therapy in non-small-cell lung cancer (NSCLC): current status and future perspectives*. Cancer Immunology, Immunotherapy, 2021. **70**(3): p. 619-631.
33. Zhang, Y., et al., *Phase I clinical trial of EGFR-specific CAR-T cells generated by the piggyBac transposon system in advanced relapsed/refractory non-small cell lung cancer patients*. J Cancer Res Clin Oncol, 2021. **147**(12): p. 3725-3734.
34. Giuffrida, L., et al., *CRISPR/Cas9 mediated deletion of the adenosine A2A receptor enhances CAR T cell efficacy*. Nature Communications, 2021. **12**(1).
35. Líndez, A.-A.M., et al., *Mitochondrial arginase-2 is a cell-autonomous regulator of CD8+ T cell function and antitumor efficacy*. JCI Insight, 2019. **4**(24).
36. Kumar, J., et al., *Deletion of Cbl-b inhibits CD8 T-cell exhaustion and promotes CAR T-cell function*. Journal for ImmunoTherapy of Cancer, 2021. **9**(1): p. e001688.
37. Alotaibi, F., et al., *CD5 blockade enhances ex vivo CD8+ T cell activation and tumour cell cytotoxicity*. European Journal of Immunology, 2020. **50**(5): p. 695-704.
38. Shi, L., et al., *CRISPR knock out CTLA-4 enhances the anti-tumor activity of cytotoxic T lymphocytes*. Gene, 2017. **636**: p. 36-41.
39. Pedicord, V.A., et al., *Single dose of anti–CTLA-4 enhances CD8 + T-cell memory formation, function, and maintenance*. Proceedings of the National Academy of Sciences, 2011. **108**(1): p. 266-271.
40. Riese, M.J., et al., *Enhanced Effector Responses in Activated CD8+ T Cells Deficient in Diacylglycerol Kinases*. Cancer Research, 2013. **73**(12): p. 3566-3577.
41. Yamamoto, T.N., et al., *T cells genetically engineered to overcome death signaling enhance adoptive cancer immunotherapy*. Journal of Clinical Investigation, 2019. **129**(4): p. 1551-1565.
42. Si, J., et al., *Hematopoietic Progenitor Kinase1 (HPK1) Mediates T Cell Dysfunction and Is a Druggable Target for T Cell-Based Immunotherapies*. Cancer Cell, 2020. **38**(4): p. 551-566 e11.
43. Good, C.R., et al., *An NK-like CAR T cell transition in CAR T cell dysfunction*. Cell, 2021. **184**(25): p. 6081-6100.e26.
44. Shang, K., et al., *Gene silencing of indoleamine 2,3-dioxygenase 1 inhibits lung cancer growth by suppressing T-cell exhaustion*. Oncology Letters, 2020.
45. Senz, A., et al. *P06.05 IDO1-deleted CAR T cells show improved therapeutic efficacy in murine pancreatic cancer models*. BMJ Publishing Group Ltd.
46. Wang, D., et al., *CRISPR Screening of CAR T Cells and Cancer Stem Cells Reveals Critical Dependencies for Cell-Based Therapies*. Cancer Discovery, 2021. **11**(5): p. 1192-1211.
47. Lukhele, S., et al., *The transcription factor IRF2 drives interferon-mediated CD8(+) T cell exhaustion to restrict anti-tumor immunity*. Immunity, 2022. **55**(12): p. 2369-2385 e10.
48. Liu, X., et al., *Genome-wide analysis identifies NR4A1 as a key mediator of T cell dysfunction*. Nature, 2019. **567**(7749): p. 525-529.
49. Chen, J., et al., *NR4A transcription factors limit CAR T cell function in solid tumours*. Nature, 2019. **567**(7749): p. 530-534.
50. Jung, I.Y., et al., *BLIMP1 and NR4A3 transcription factors reciprocally regulate antitumor CAR T cell stemness and exhaustion*. Sci Transl Med, 2022. **14**(670): p. eabn7336.

51. Janelle, V., et al., *p16(INK4a) Regulates Cellular Senescence in PD-1-Expressing Human T Cells*. Front Immunol, 2021. **12**: p. 698565.
52. Gurusamy, D., et al., *Multi-phenotype CRISPR-Cas9 Screen Identifies p38 Kinase as a Target for Adoptive Immunotherapies*. Cancer Cell, 2020. **37**(6): p. 818-833 e9.
53. Ye, L., et al., *In vivo CRISPR screening in CD8 T cells with AAV–Sleeping Beauty hybrid vectors identifies membrane targets for improving immunotherapy for glioblastoma*. Nature Biotechnology, 2019. **37**(11): p. 1302-1313.
54. Yoshikawa, T., et al., *Genetic ablation of PRDM1 in antitumor T cells enhances therapeutic efficacy of adoptive immunotherapy*. Blood, 2022. **139**(14): p. 2156-2172.
55. Wiede, F., et al., *PTP1B Is an Intracellular Checkpoint that Limits T-cell and CAR T-cell Antitumor Immunity*. Cancer Discov, 2022. **12**(3): p. 752-773.
56. Wiede, F., et al., *PTPN2 phosphatase deletion in T cells promotes anti-tumour immunity and CAR T-cell efficacy in solid tumours*. The EMBO Journal, 2020. **39**(2).
57. Carnevale, J., et al., *RASA2 ablation in T cells boosts antigen sensitivity and long-term function*. Nature, 2022. **609**(7925): p. 174-182.
58. Weisshaar, N., et al., *Rgs16 promotes antitumor CD8(+) T cell exhaustion*. Sci Immunol, 2022. **7**(71): p. eabh1873.
59. Olesch, C., et al., *S1PR4 ablation reduces tumor growth and improves chemotherapy via CD8+ T cell expansion*. J Clin Invest, 2020. **130**(10): p. 5461-5476.
60. Trefny, M.P., et al., *Deletion of SNX9 alleviates CD8 T cell exhaustion for effective cellular cancer immunotherapy*. Nat Commun, 2023. **14**(1): p. 86.
61. Jain, N., et al., *SUV39H1 disruption imparts functional persistence to CD28-costimulated human CAR T cells*. The Journal of Immunology, 2022. **208**(Supplement_1): p. 122.05-122.05.
62. Lopez-Cobo, S., et al., *SUV39H1 Ablation Enhances Long-term CAR T Function in Solid Tumors*. Cancer Discov, 2024. **14**(1): p. 120-141.
63. Tang, N., et al., *TGF-β inhibition via CRISPR promotes the long-term efficacy of CAR T cells against solid tumors*. JCI Insight, 2020. **5**(4).
64. Jackson, Z., et al., *Sequential Single-Cell Transcriptional and Protein Marker Profiling Reveals TIGIT as a Marker of CD19 CAR-T Cell Dysfunction in Patients with Non-Hodgkin Lymphoma*. Cancer Discov, 2022. **12**(8): p. 1886-1903.
65. Seo, H., et al., *TOX and TOX2 transcription factors cooperate with NR4A transcription factors to impose CD8*

+

T cell exhaustion. Proceedings of the National Academy of Sciences, 2019. **116**(25): p. 12410-12415.
66. Song, M., et al., *IRE1α–XBP1 controls T cell function in ovarian cancer by regulating mitochondrial activity*. Nature, 2018. **562**(7727): p. 423-428.
67. Mai, D., et al., *Combined disruption of T cell inflammatory regulators Regnase-1 and Roquin-1 enhances antitumor activity of engineered human T cells*. Proceedings of the National Academy of Sciences, 2023. **120**(12).
68. Gargett, T. and M.P. Brown, *The inducible caspase-9 suicide gene system as a â€œsafety switchâ€ to limit on-target, off-tumor toxicities of chimeric antigen receptor T cells*. Frontiers in Pharmacology, 2014. **5**.
69. Hinrichs, C.S., et al., *Adoptively transferred effector cells derived from naïve rather than central memory CD8+ T cells mediate superior antitumor immunity*. Proceedings of the National Academy of Sciences, 2009. **106**(41): p. 17469-17474.
70. Gattinoni, L., et al., *A human memory T cell subset with stem cell-like properties*. Nat Med, 2011. **17**(10): p. 1290-7.

71. Salter, A.I., et al., *Comparative analysis of TCR and CAR signaling informs CAR designs with superior antigen sensitivity and in vivo function*. Sci Signal, 2021. **14**(697).
72. Wu, L., et al., *Signaling from T cell receptors (TCRs) and chimeric antigen receptors (CARs) on T cells*. Cell Mol Immunol, 2020. **17**(6): p. 600-612.
73. Zhao, Z., et al., *Structural Design of Engineered Costimulation Determines Tumor Rejection Kinetics and Persistence of CAR T Cells*. Cancer Cell, 2015. **28**(4): p. 415-428.
74. Cappell, K.M. and J.N. Kochenderfer, *A comparison of chimeric antigen receptors containing CD28 versus 4-1BB costimulatory domains*. Nat Rev Clin Oncol, 2021. **18**(11): p. 715-727.
75. Philipson, B.I., et al., *4-1BB costimulation promotes CAR T cell survival through noncanonical NF-kappaB signaling*. Sci Signal, 2020. **13**(625).
76. Simula, L., et al., *Mitochondrial metabolism sustains CD8(+) T cell migration for an efficient infiltration into solid tumors*. Nat Commun, 2024. **15**(1): p. 2203.
77. LaFleur, M.W., et al., *A CRISPR-Cas9 delivery system for in vivo screening of genes in the immune system*. Nature Communications, 2019. **10**(1).
78. Kallies, A., D. Zehn, and D.T. Utzschneider, *Precursor exhausted T cells: key to successful immunotherapy?* Nat Rev Immunol, 2020. **20**(2): p. 128-136.
79. Zheng, W., et al., *Regnase-1 suppresses TCF-1+ precursor exhausted T-cell formation to limit CAR–T-cell responses against ALL*. Blood, 2021. **138**(2): p. 122-135.
80. Si, X., et al., *Preclinical Evaluation of CAR T Cell Function: In Vitro and In Vivo Models*. International Journal of Molecular Sciences, 2022. **23**(6): p. 3154.
81. Arunachalam, A.K., et al., *Advancing CAR T-cell therapies: Preclinical insights and clinical translation for hematological malignancies*. Blood Rev, 2024. **68**: p. 101241.
82. Stribbling, S.M., C. Beach, and A.J. Ryan, *Orthotopic and metastatic tumour models in preclinical cancer research*. Pharmacol Ther, 2024. **257**: p. 108631.
83. Melssen, M.M., et al., *Barriers to immune cell infiltration in tumors*. Journal for ImmunoTherapy of Cancer, 2023. **11**(4): p. e006401.
84. Donnadieu, E., et al., *Surmounting the obstacles that impede effective CAR T cell trafficking to solid tumors*. Journal of Leukocyte Biology, 2020. **108**(4): p. 1067-1079.
85. Katz, S.C., et al., *Phase I Hepatic Immunotherapy for Metastases Study of Intra-Arterial Chimeric Antigen Receptor–Modified T-cell Therapy for CEA+ Liver Metastases*. Clinical Cancer Research, 2015. **21**(14): p. 3149-3159.
86. Zhao, Y., et al., *IL-10-expressing CAR T cells resist dysfunction and mediate durable clearance of solid tumors and metastases*. Nat Biotechnol, 2024. **42**(11): p. 1693-1704.
87. Hou, A.J., L.C. Chen, and Y.Y. Chen, *Navigating CAR-T cells through the solid-tumour microenvironment*. Nat Rev Drug Discov, 2021. **20**(7): p. 531-550.
88. Schurich, A., I. Magalhaes, and J. Mattsson, *Metabolic regulation of CAR T cell function by the hypoxic microenvironment in solid tumors*. Immunotherapy, 2019. **11**(4): p. 335-345.
89. Andreu-Saumell, I., et al., *CAR affinity modulates the sensitivity of CAR-T cells to PD-1/PD-L1-mediated inhibition*. Nature Communications, 2024. **15**(1).
90. Korell, F., et al., *In vivo CRISPR screens identify key modifiers of CAR T cell function in myeloma*. bioRxiv preprint, 2024.
91. Bloh, K., et al., *Deconvolution of Complex DNA Repair (DECODR): Establishing a Novel Deconvolution Algorithm for Comprehensive Analysis of CRISPR-Edited Sanger Sequencing Data*. The CRISPR Journal, 2021. **4**(1): p. 120-131.
92. Cash, W., *Parameter estimation in astronomy through application of the likelihood ratio*. The Astrophysical Journal, 1979. **228**: p. 939.
93. Simoni, Y., et al., *Human Innate Lymphoid Cell Subsets Possess Tissue-Type Based Heterogeneity in Phenotype and Frequency*. Immunity, 2018. **48**(5): p. 1060.
94. Simoni, Y., et al., *Bystander CD8(+) T cells are abundant and phenotypically distinct in human tumour infiltrates*. Nature, 2018. **557**(7706): p. 575-579.

95. Li, S., et al., *Bystander CD4 + T cells infiltrate human tumors and are phenotypically distinct*. OncoImmunology, 2022. **11**(1).
96. Moore, W.A. and D.R. Parks, *Update for the logicle data scale including operational code implementations*. Cytometry Part A, 2012. **81A**(4): p. 273-277.

ACKNOWLEDGEMENTS

This work was supported by INSERM, the French Ligue Nationale Contre le Cancer (LNCC), the Cochin Institute (POC 2020 and 2025, PIC 2025), Inserm Transfert (CoPOC), Université Paris Cité (Ami-Stratex 2024), and the Laboratory of Excellence GR-EX. M.F. and D.A. were supported by PhD fellowships from the Ligue Nationale Contre le Cancer and the China Scholarship Council (CSC), respectively. M.F. also received support from the "EUR G.E.N.E Fellowship" during his Master's internship.

We are extremely grateful to the members of the following platforms and facilities: the Cochin Institute Imaging Facility (IMAG'IC); the Cytometry and Immunobiology Platform (CYBIO), with special thanks to Youcef Hadjou and Sougnaya Many; the Histology, Immunostaining, and Microdissection Facility (HistIM), especially Maryline Favier, Fabiola Ely-Marius, and Rachel Onifarasoaniaina; and the In Vivo Imaging Facility (PIV), with special thanks to Gilles Renault, Isabelle Lagoutte, Franck Lager, Pierre Monbernard, and Giovanna Bibaki.

We thank Pierre de la Grange (Genosplice) and Olivier Tenaillon for helpful discussions on the interpretation of statistical analyses, and Jaques Dutrieux for his help on the set up of the PCR protocols. We are also grateful to Concetta Quintarelli, Simona Manni, Beatrice Mezzopra, Julien Sage, Isabelle Munoz, and Marianne Mangeney for their valuable scientific input.

Finally, we thank all members of the "Cancer Immunotherapy and Cell Reprogramming" and "Cancer and Immune Response" teams, especially Alice Machado, Marwan Fontaine, Jeane Pitiot and Irena Rajnpreht, for their daily support and constructive scientific feedback.

AUTHOR CONTRIBUTIONS

Conceptualization & Writing – Original Draft: M.F. and F.P.
Funding Acquisition and Resources: F.P., N.B., and E.D.
Investigation: M.F., D.A., C.C., L.S., L.A., Y.S., M.C.-A.G., A.V., A.V., M.M., J.M., N.T., N.B., and E.D.
Writing – Review & Editing: N.T., J.M., N.B., and E.D.
All authors read and approved the final manuscript.

COMPETING INTERESTS

The authors declare no competing interests. M.F., D.A., E.D., and F.P. are co-inventors on a patent filed by Inserm Transfert, the technology transfer office for INSERM, CNRS, and Université Paris Cité.

MATERIALS AND CORRESPONDENCE

Frederic Pendino and Mattia Fumagalli

Figure 1

A

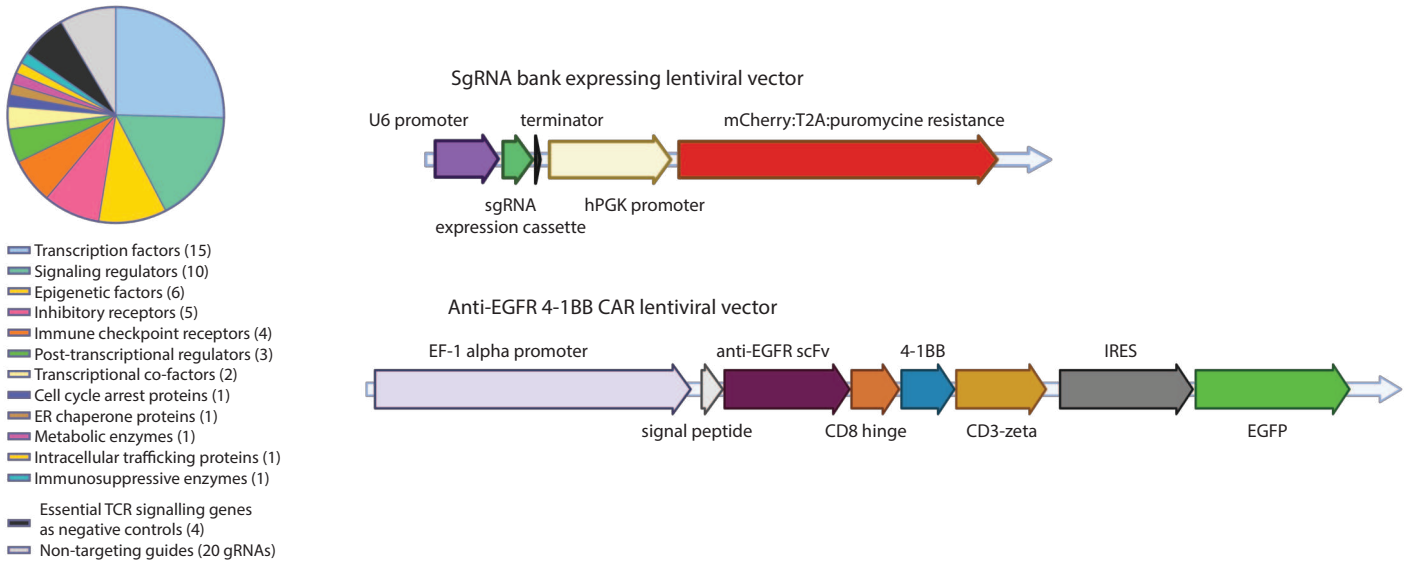

B

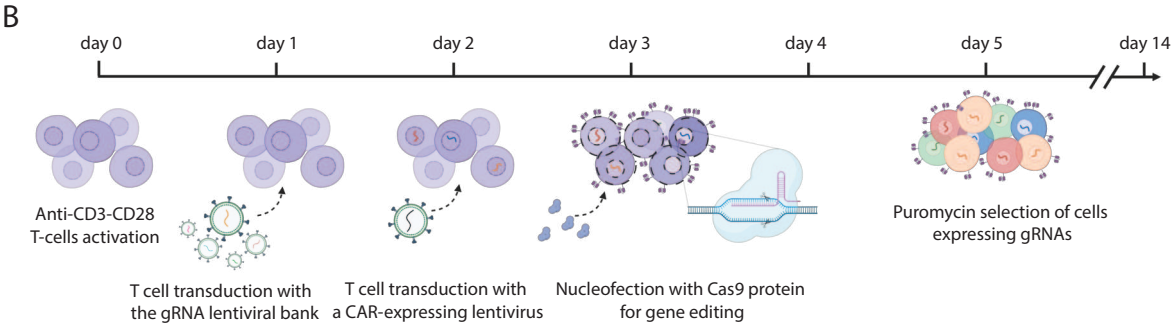

C

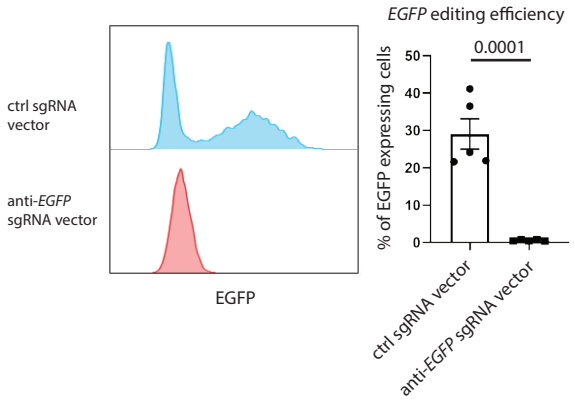

D

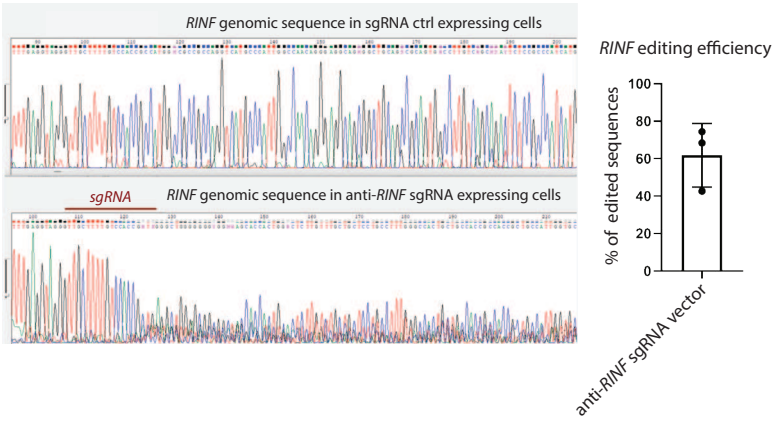

E

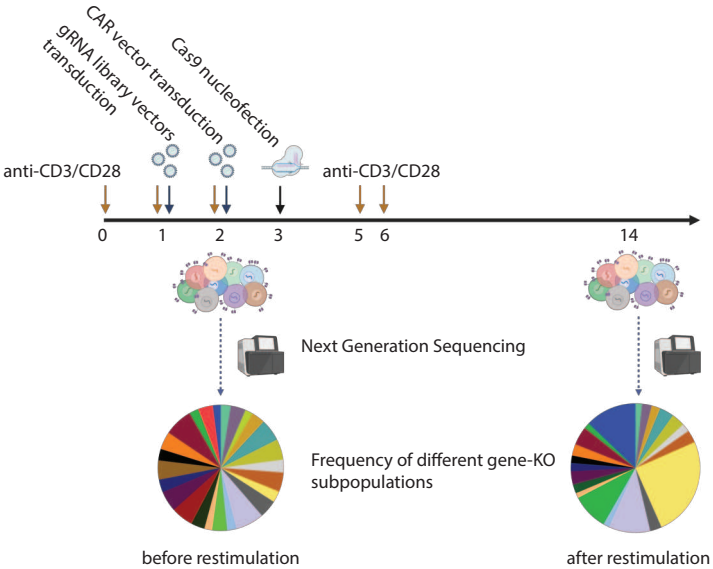

F

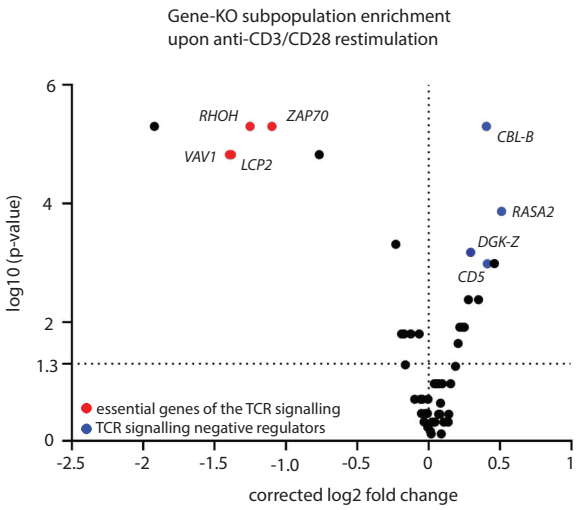

Figure 1. Description and validation of our CRISPR/Cas9 library: **(A) (left)** SgRNA bank composition, each of the 50 target genes and the 4 essential negative control genes is targeted by 4 guide RNAs, 20 non-targeting sgRNAs have been added as baseline control. **(right)** Schematics of lentiviral vectors expressing the sgRNA bank and the CAR construct. **(B)** CAR-T cells editing strategy schematics. **(C)** Validation of gene editing strategy by a pilot system targeting *EGFP* in EGFP expressing T cells, as evaluated by signal loss upon knock out trough flow cytometry. p-value of unpaired t-test. **(D)** Validation of gene editing strategy by a pilot system targeting the gene *RINF* in T cells, as evaluated by proportion of modified genomic sequences upon knock out, determined through sanger sequencing and deconvolution analysis of chromatograms files. **(E)** schematics of the in vitro expansion experiment for gRNA library validation **(F)** gene-KO subpopulations frequency variations from library transduction to the end of in vitro expansion assay, genes essential for TCR signalling, used as negative control genes are highlighted in red and TCR signalling negative regulators are in blue. log2 fold change for each gene, expressing frequency changes between the two time points, is corrected to average log2 fold change for 20 non-targeting gRNA. (n=2 biological replicates)

Figure 2

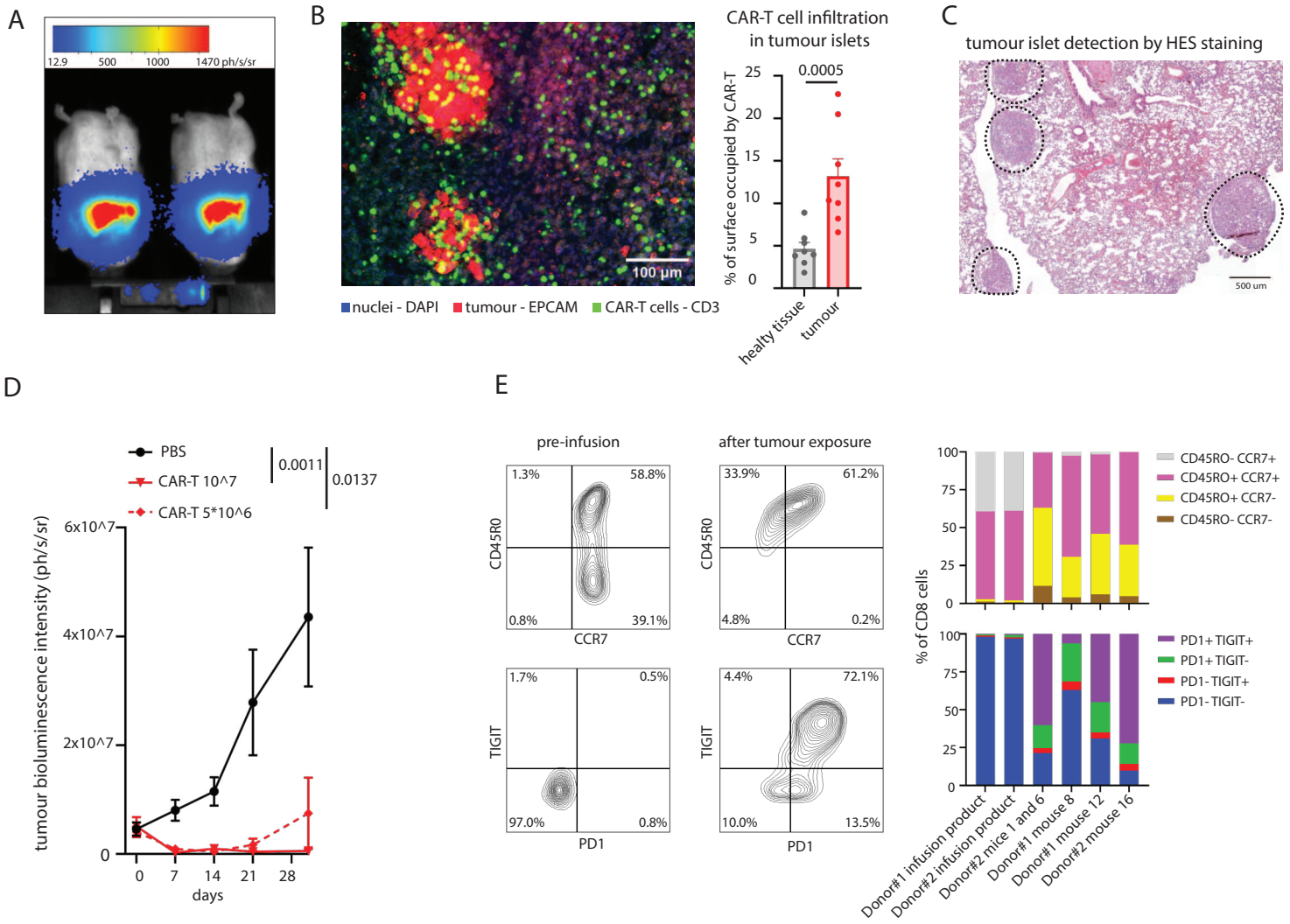
A
12.9
500
1000
1470 ph/s/sr
B
100 µm
nuclei - DAPI
tumour - EPCAM
CAR-T cells - CD3
CAR-T cell infiltration in tumour islets
0.0005
% of surface occupied by CAR-T
healty tissue
tumour
C
tumour islet detection by HES staining
500 um
D
PBS
CAR-T 10^7
CAR-T 5*10^6
0.0011
0.0137
tumour bioluminescence intensity (ph/s/sr)
6x10^7
4x10^7
2x10^7
0
days
E
pre-infusion
after tumour exposure
CD45RO
CCR7
TIGIT
PD1
1.3%
58.8%
0.8%
39.1%
33.9%
61.2%
4.8%
0.2%
1.7%
0.5%
97.0%
0.8%
4.4%
72.1%
10.0%
13.5%
% of CD8 cells
CD45RO- CCR7+
CD45RO+ CCR7+
CD45RO+ CCR7-
CD45RO- CCR7-
PD1+ TIGIT+
PD1+ TIGIT-
PD1- TIGIT+
PD1- TIGIT-
Donor#1 infusion product
Donor#2 infusion product
Donor#2 mice 1 and 6
Donor#1 mouse 8
Donor#1 mouse 12
Donor#2 mouse 16
F
A549 cells only
A549 cells + CAR-T cells infusion product
A549 cells + CAR-T cells extracted from tumours
0h
24h
Cytotoxicity
no treatment
CAR-T cells infusion product
CAR-T cells extracted from tumours
% of A549 mcherry+ cells confluence
0.0060
0.0411
Proliferation
CAR-T cells infusion product
CAR-T cells extracted from tumours
millions of cells
<0.0001
G
mice data at endpoint
power law fit
y= (4.8*10^6)*x^(-0.86)
ph/s/sr
% of CAR-T
log10 ph/s/sr
log10 % of CAR-T

Figure 2. The A549 orthotopic model is a pertinent model of solid tumour for studying CAR-T cells therapy persistence and efficacy: **(A)** Exemplary bioluminescence live imaging of A549 cells orthotopic lung tumour. **(B)** Exemplary Immunofluorescence microscopy image of A549 cells (EpCAM staining in red) tumour islet in mice lung, with CAR-T infiltrate (human CD3 staining cells in green). Infiltration analysis has been performed on tumour bearing lung slices images (n=8), 4 days post CAR-T cells injection. P-values are calculated by one-way ANOVA test. **(C)** Exemplary Haematoxylin Eosin staining (HES) of lung tumour section. **(D)** Tumour growth curve, assessed by bioluminescence analysis, in mice receiving mock solution (n=5) or treated with 10^7 CAR-T cells(n=3) or 5*10^6 CAR-T cells(n=5). P-values are calculated by two-ways ANOVA test and results for whole curves comparisons are shown. **(E)** Phenotypical characterisation of CAR-T cells by flow cytometry. We compared CAR-T cells from infusion products and CAR-T cells recovered from mice which received the 5*10^6 dose after long term exposure to tumour *in vivo*. **(F)** Functional characterisation CAR-T cells from infusion products and CAR-T cells recovered from mice. Cytotoxic capacity was assessed by calculating surface reduction of mCherry+ tumour cells when co-cultured with CAR-T cells, at least 3 images were taken per condition, at each time point. Proliferation capacity was assessed by cell counting upon 7 days after anti-CD3/C28 stimulation (n=3 biological replicates for pre-infusion CAR-T cells, n=4 for mice extracted CAR-T cells). P-values are calculated by two-ways ANOVA test, results for final time point comparisons are shown. **(G) (left)** Power-law defined negative correlation among tumour mass, assessed by bioluminescence, and % of CAR-T cells in mice lung at the experiment endpoint. Data shown are collected from all screening experiments performed. The represented power law has been defined through data fitting. (right) representation of the same data and fitting curve on log10 axes.

Figure 3

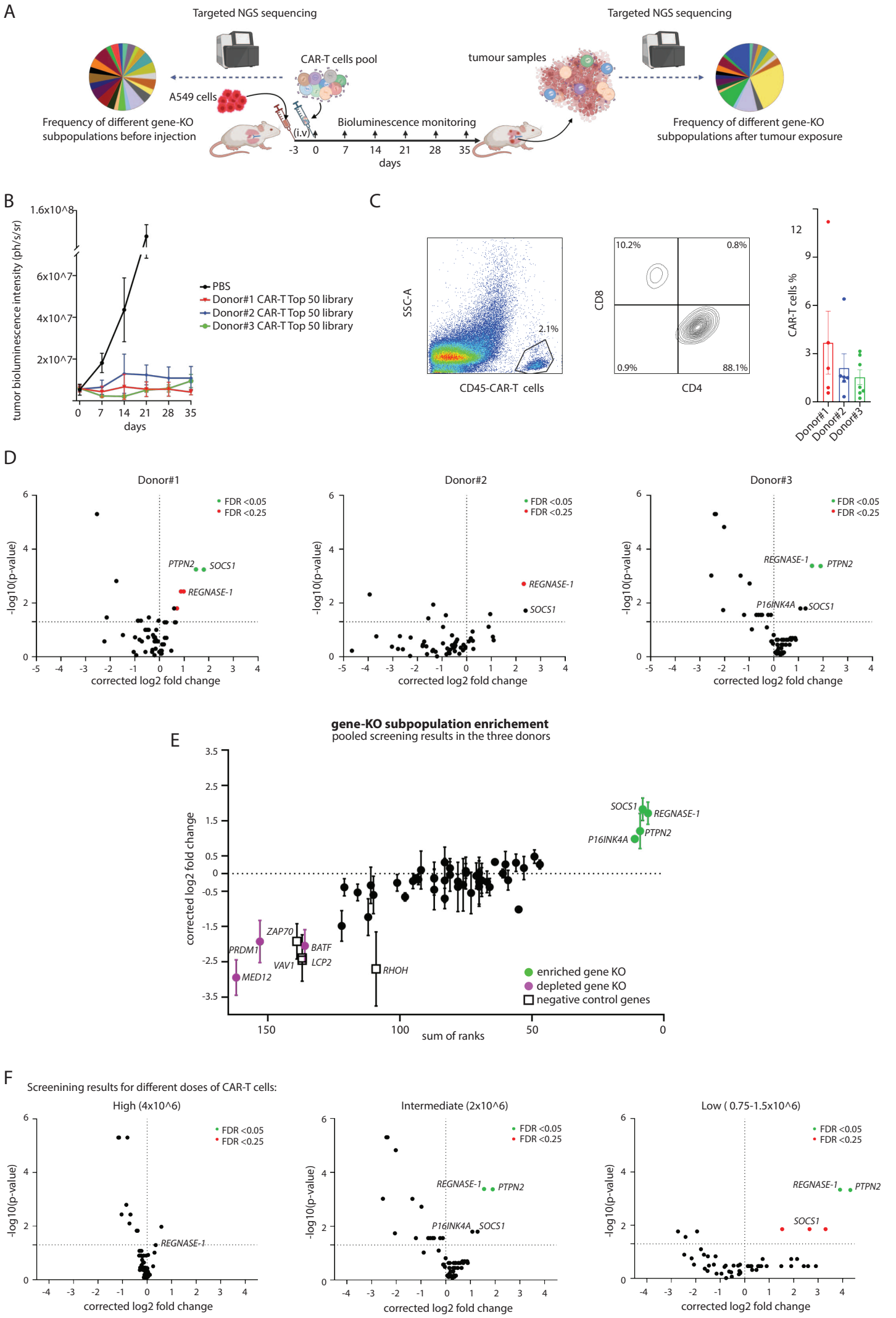
A
Targeted NGS sequencing
CAR-T cells pool
A549 cells
Frequency of different gene-KO subpopulations before injection
(i.v)
Bioluminescence monitoring
-3 0 7 14 21 28 35
days
tumour samples
Targeted NGS sequencing
Frequency of different gene-KO subpopulations after tumour exposure
B
tumor bioluminescence intensity (ph/s/sr)
1.6x10^8
6x10^7
4x10^7
2x10^7
0 7 14 21 28 35
days
PBS
Donor#1 CAR-T Top 50 library
Donor#2 CAR-T Top 50 library
Donor#3 CAR-T Top 50 library
C
SSC-A
2.1%
CD45-CAR-T cells
CD8
10.2%
0.8%
0.9%
88.1%
CD4
CAR-T cells %
Donor#1
Donor#2
Donor#3
D
Donor#1
Donor#2
Donor#3
FDR <0.05
FDR <0.25
-log10(p-value)
corrected log2 fold change
PTPN2
SOCS1
REGNASE-1
P16INK4A
E
gene-KO subpopulation enrichement
pooled screening results in the three donors
corrected log2 fold change
sum of ranks
SOCS1
REGNASE-1
PTPN2
P16INK4A
ZAP70
PRDM1
BATF
VAV1
LCP2
MED12
RHOH
enriched gene KO
depleted gene KO
negative control genes
F
Screenining results for different doses of CAR-T cells:
High (4x10^6)
Intermediate (2x10^6)
Low (0.75-1.5x10^6)
FDR <0.05
FDR <0.25
-log10(p-value)
corrected log2 fold change
REGNASE-1
PTPN2
P16INK4A
SOCS1

Figure 3. ***In vivo*** **screening in the orthotopic tumour model unveils 4 most promising gene KO strategies**: **(A)** Schematics of the experiment. **(B)** Tumour growth curve as determined by bioluminescence for mice treated either with excipient (n=5) or 2*10^6 CAR-T modified with our Top 50 library of lentiviral bank, from three different Donors #1 (n=6), #2 (n=6), #3 (n=7) **(C)** CAR-T cells detection in mice lungs by flow cytometry. For CAR-T cells from donor #1, mouse 24 data were collected at anticipated sacrifice at 28 days **(D)** Screening results for CAR-T cells from the three different donors, gene-ko subpopulation proportions are compared in mice lungs at the endpoint of the experiment vs in infusion products. Log2 fold change for each gene, expressing frequency changements between the two time points, is corrected to average log2 fold change for 20 non-targeting gRNA. P-values are determined by MAGeCK permutation test and False Discovery Rate (FDR) values are calculated with Benjamini-Hochberg correction. **(E)** Overall results pooling the three independent screenings, log2 fold change for each gene is calculated as average of these values from each screening. Sum of rank value is determined as sum of the rankings assigned by MAGeCK alpha-RRA algorithm for each gene in the three screenings. **(F)** Screening results from three different experiments in which either 4*10^6 CAR-T Top 50 library, 2*10^6 CAR-T Top 50 library or 0.75-1.5*10^6 CAR-T Top 50 library were injected to mice, with progressively less effective tumour control, and therefore increasing selective pressure on CAR-T cells. Gene-ko subpopulation proportions are compared in mice lungs at the endpoint of the experiment vs in infusion products. Log2 fold change for each gene, expressing frequency changes between the two time points, is corrected to average log2 fold change for 20 non-targeting gRNA. P-values are determined by MAGeCK permutation test and FDR values are calculated with Benjamini-Hochberg correction.

Figure 4

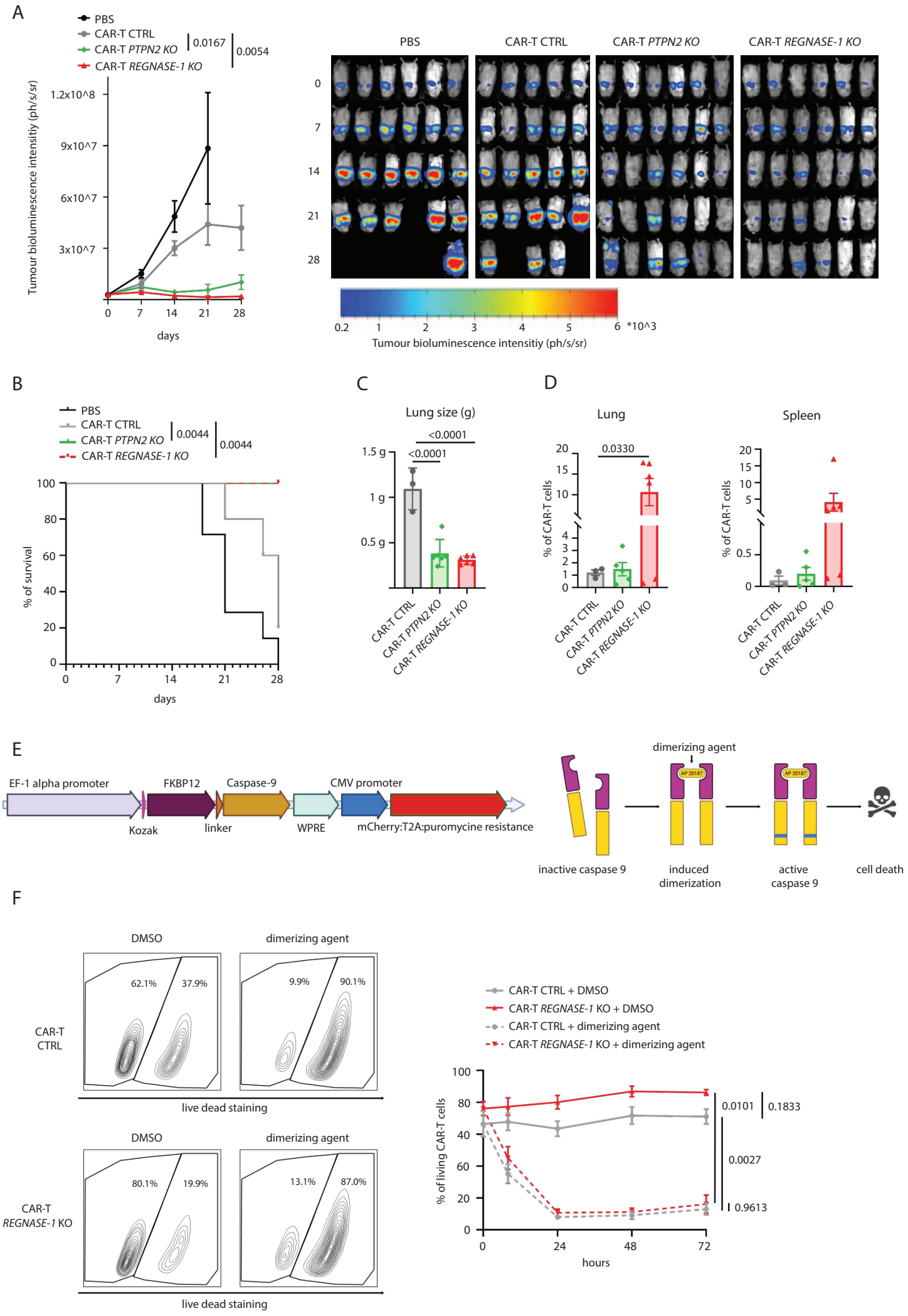
A
PBS
CAR-T CTRL
CAR-T PTPN2 KO
CAR-T REGNASE-1 KO
0.0167
0.0054
Tumour bioluminescence intensitiy (ph/s/sr)
1.2x10^8
9x10^7
6x10^7
3x10^7
0
7
14
21
28
days
PBS
CAR-T CTRL
CAR-T PTPN2 KO
CAR-T REGNASE-1 KO
0.2
1
2
3
4
5
6
*10^3
Tumour bioluminescence intensitiy (ph/s/sr)
B
PBS
CAR-T CTRL
CAR-T PTPN2 KO
CAR-T REGNASE-1 KO
0.0044
0.0044
% of survival
100
80
60
40
20
0
days
C
Lung size (g)
<0.0001
<0.0001
1.5 g
1 g
0.5 g
CAR-T CTRL
CAR-T PTPN2 KO
CAR-T REGNASE-1 KO
D
Lung
Spleen
0.0330
% of CAR-T cells
CAR-T CTRL
CAR-T PTPN2 KO
CAR-T REGNASE-1 KO
E
EF-1 alpha promoter
FKBP12
Caspase-9
CMV promoter
Kozak
linker
WPRE
mCherry:T2A:puromycine resistance
dimerizing agent
AP 20187
inactive caspase 9
induced dimerization
active caspase 9
cell death
F
DMSO
dimerizing agent
CAR-T CTRL
62.1%
37.9%
9.9%
90.1%
live dead staining
CAR-T REGNASE-1 KO
80.1%
19.9%
13.1%
87.0%
live dead staining
CAR-T CTRL + DMSO
CAR-T REGNASE-1 KO + DMSO
CAR-T CTRL + dimerizing agent
CAR-T REGNASE-1 KO + dimerizing agent
% of living CAR-T cells
0.0101
0.1833
0.0027
0.9613
0
24
48
72
hours

Figure 4. **Validation of top targeting genes *REGNASE-1* and *PTPN2* KO CAR-T cell improved antitumour efficacy**: **(A)** Tumour growth curve in mice treated either with excipient (n=6), 10^6 CTRL CAR-T cells (n=5), 10^6 *PTPN2* KO CAR-T cells (n=6) or 10^6 *REGNASE-1* KO CAR-T cells (n=6). p-values are calculated by two-ways ANOVA test, results for whole curves comparisons are shown. Individual images for each mouse at different time points on the right. **(B)** Survival curves for mice treated with the aforementioned conditions. P-values have been determined by log-rank mantel-cox test. **(C)** Lung size at endpoint, indicative of tumour mass, p-values are calculated by one-way ANOVA test. **(D)** % of CAR-T cells in lungs and spleens of mice at the endpoint as determined by flow cytometry. **(E)** We equipped CAR-T cells with a vector expressing human CASPASE-9 fused with FK506-binding protein 12 (with F36V mutation), to allow dimerization upon administration of the dimerizing agent AP02187, leading to cell death. Unmodified CAR-T cells (n=3) are compared to *REGNASE-1* KO CAR-T cells (n=3). **(F)** Cell death was determined by flow cytometry analysis with live-dead blue dye, data are corrected to cells numbers, to account for dead cell lysis. P-values are calculated by two-ways ANOVA test, results for final time point are shown.

Figure 5

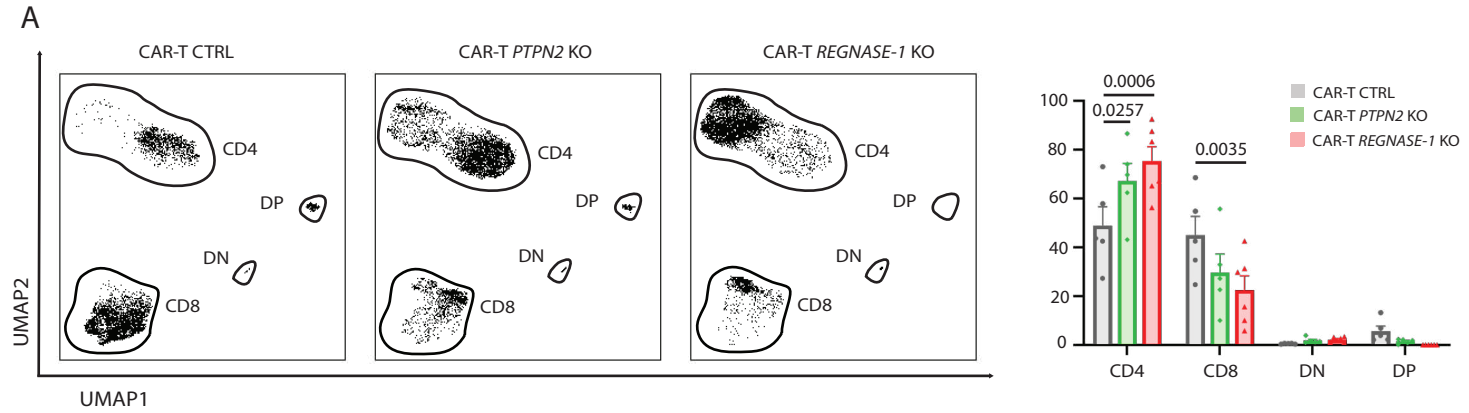
A
CAR-T CTRL
CAR-T PTPN2 KO
CAR-T REGNASE-1 KO
CD4
DP
DN
CD8
UMAP2
UMAP1
0.0006
0.0257
0.0035
CAR-T CTRL
CAR-T PTPN2 KO
CAR-T REGNASE-1 KO
CD4
CD8
DN
DP

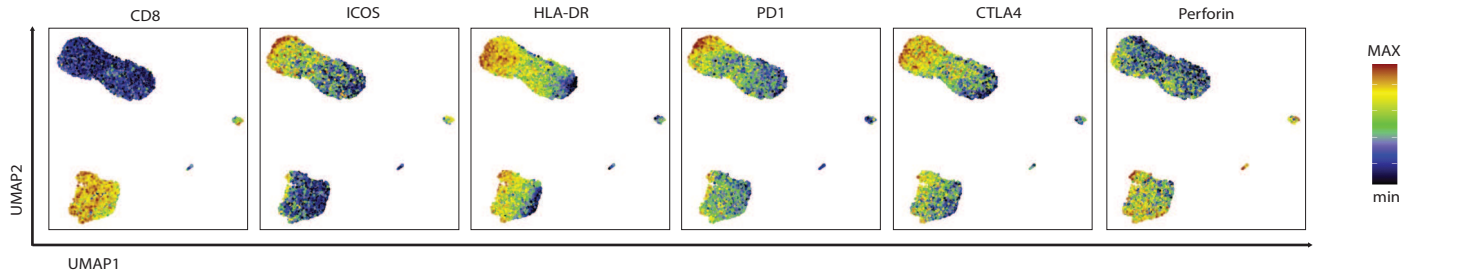
CD8
ICOS
HLA-DR
PD1
CTLA4
Perforin
MAX
min
UMAP2
UMAP1

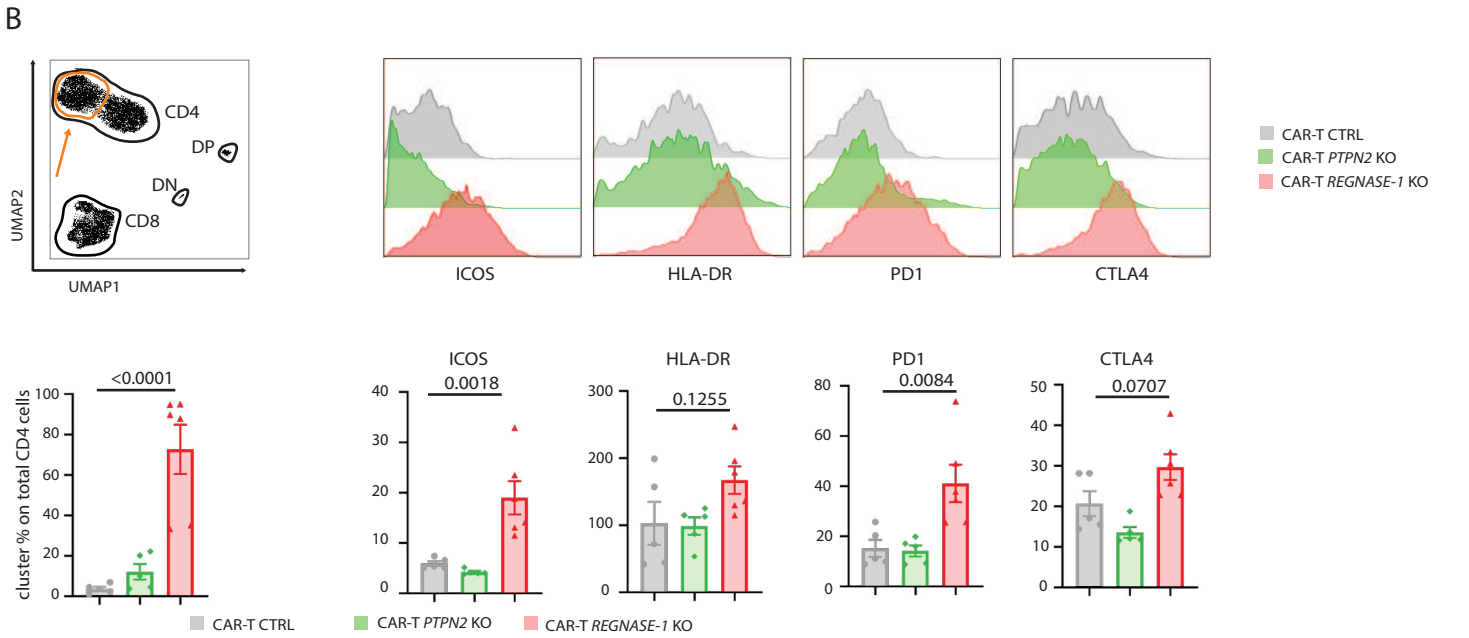
B
CD4
DP
DN
CD8
UMAP2
UMAP1
ICOS
HLA-DR
PD1
CTLA4
CAR-T CTRL
CAR-T PTPN2 KO
CAR-T REGNASE-1 KO
<0.0001
cluster % on total CD4 cells
ICOS
0.0018
HLA-DR
0.1255
PD1
0.0084
CTLA4
0.0707
CAR-T CTRL
CAR-T PTPN2 KO
CAR-T REGNASE-1 KO

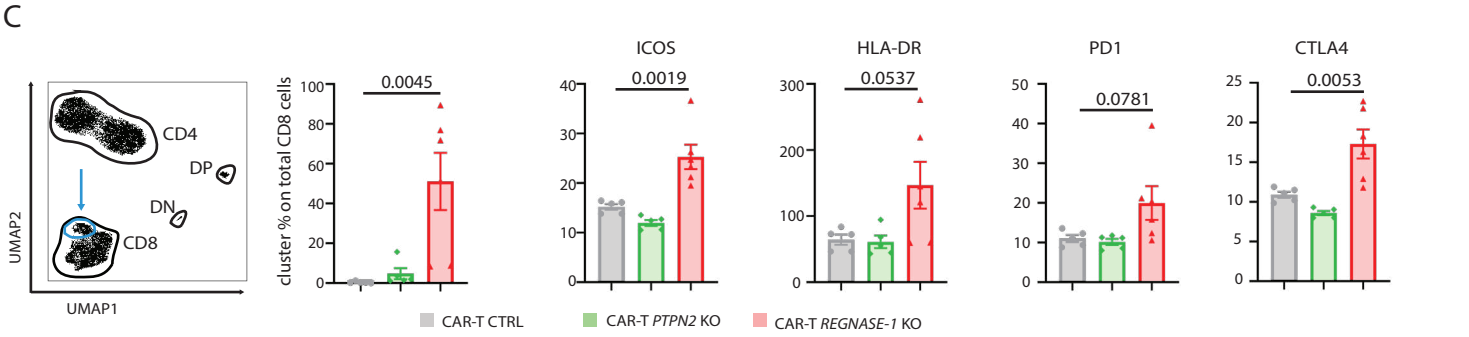
C
CD4
DP
DN
CD8
UMAP2
UMAP1
0.0045
cluster % on total CD8 cells
ICOS
0.0019
HLA-DR
0.0537
PD1
0.0781
CTLA4
0.0053
CAR-T CTRL
CAR-T PTPN2 KO
CAR-T REGNASE-1 KO

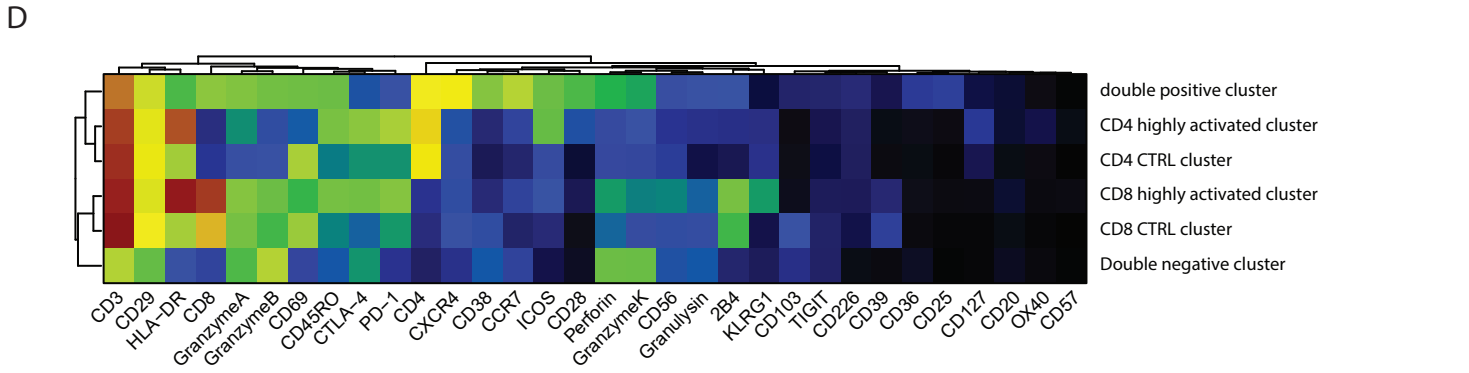
D
double positive cluster
CD4 highly activated cluster
CD4 CTRL cluster
CD8 highly activated cluster
CD8 CTRL cluster
Double negative cluster
CD3
CD29
HLA-DR
CD8
GranzymeA
GranzymeB
CD69
CD45RO
CTLA-4
PD-1
CD4
CXCR4
CD38
CCR7
ICOS
CD28
Perforin
GranzymeK
CD56
Granulysin
2B4
KLRG1
CD103
TIGIT
CD226
CD39
CD36
CD25
CD127
CD20
OX40
CD57

Figure 5. **Cytometry by Time of Flight (CyTOF) characterisation of *REGNASE-1* and *PTPN2* KO CAR-T cells in mice lung tumours**: **(A)** UMAP analysis of CyTOF data from CAR-T cells in lung tumour samples at the endpoint of the experiment. Relative proportion of main clusters (upper right) and main markers of interests (bottom) in samples from CTRL (n=5), *REGNASE-1* KO (n=6) and *PTPN2* KO (n=5) are also shown. p-values are calculated by one-way ANOVA test. **(B)** Characterisation of variations within the CD4 cluster. the formation of a sub-cluster, for the *REGNASE-1* KO condition, is shown in the combinatory graph of the three exemplary samples (top left) variations of expression for markers defining such cluster in the 3 different exemplary samples are then shown (top right). Frequency of such cluster among all samples and expression levels for the aforementioned markers are shown (respectively bottom left and bottom right) p-values are calculated by one way ANOVA test. **(C)** Characterisation of variations within the CD8 cluster. the formation of a sub-cluster, for the *REGNASE-1* KO condition, is shown in the combinatory graph of the three exemplary samples (left) overall variations of expression for markers defining such cluster in different condition are then shown (top right). Frequency of such cluster among all samples and expression levels for the aforementioned markers are shown (respectively bottom left and bottom right) p-values are calculated by one way ANOVA test. **(D)** Clustered heatmap and relative dendrogram, data are calculated as overall variation of different markers among defined clusters in all samples.

Figure 6

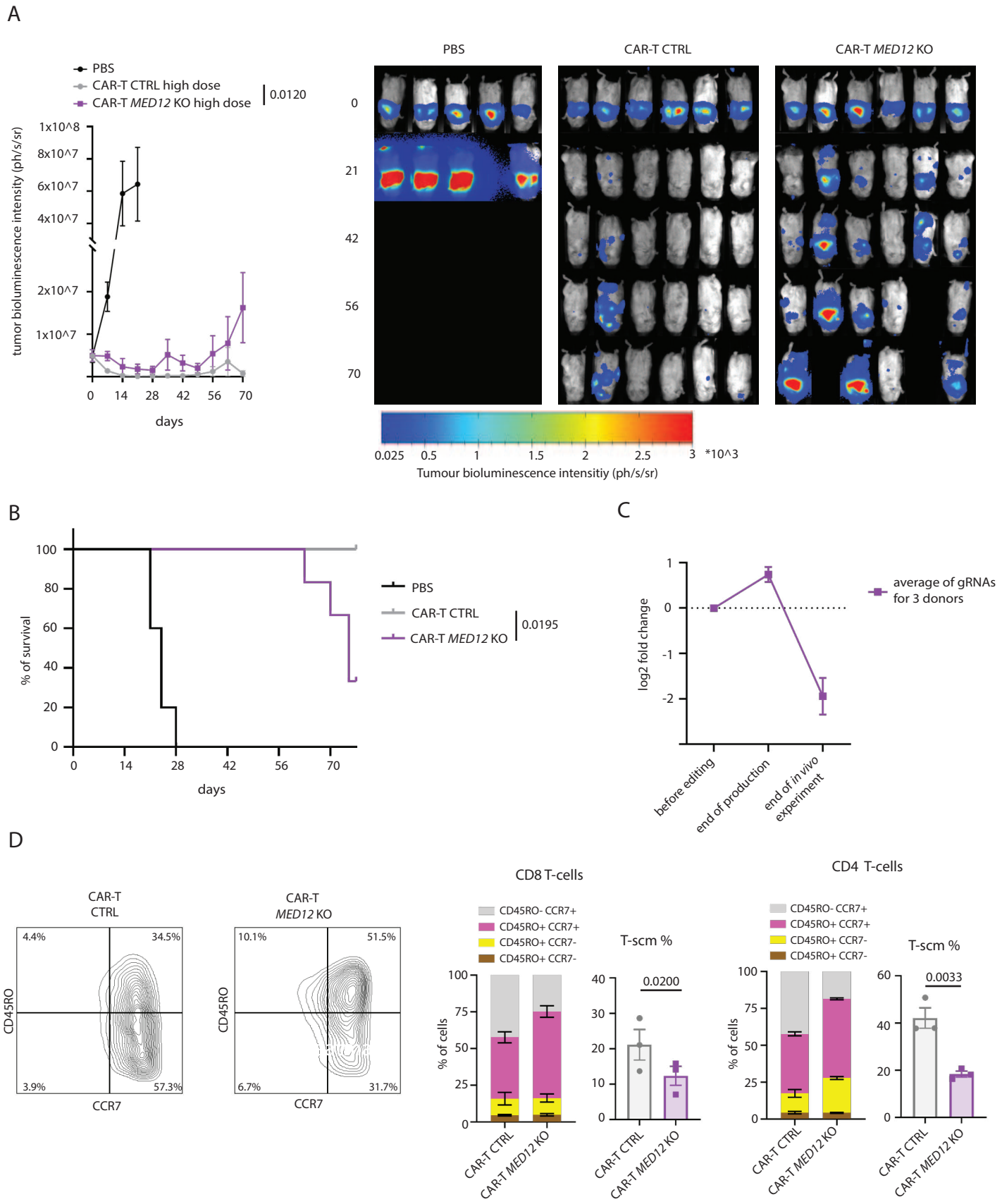
A
PBS
CAR-T CTRL high dose
CAR-T MED12 KO high dose
0.0120
tumor bioluminescence intensity (ph/s/sr)
1x10^8
8x10^7
6x10^7
4x10^7
2x10^7
1x10^7
0
14
28
42
56
70
days
PBS
CAR-T CTRL
CAR-T MED12 KO
0
21
42
56
70
0.025
0.5
1
1.5
2
2.5
3
*10^3
Tumour bioluminescence intensitiy (ph/s/sr)
B
100
80
60
40
20
0
% of survival
0
14
28
42
56
70
days
PBS
CAR-T CTRL
CAR-T MED12 KO
0.0195
C
1
0
-1
-2
log2 fold change
average of gRNAs for 3 donors
before editing
end of production
end of in vivo experiment
D
CAR-T CTRL
CAR-T MED12 KO
4.4%
34.5%
3.9%
57.3%
10.1%
51.5%
6.7%
31.7%
CD45RO
CCR7
CD8 T-cells
CD4 T-cells
CD45RO- CCR7+
CD45RO+ CCR7+
CD45RO+ CCR7-
CD45RO+ CCR7-
% of cells
T-scm %
0.0200
0.0033
CAR-T CTRL
CAR-T MED12 KO

Figure 6. **Study of the effects of *MED12* KO on CAR-T cells *in vitro* proliferation and differentiation and *in vivo* efficacy against lung adenocarcinoma**: **(A)** Tumour growth curve in mice treated either with excipient (n=5), 3*10^6 CTRL CAR-T cells (n=6) or 3*10^6 *MED12* KO CAR-T cells (n=6). In reason of the great disparity of signal within mice of the same groups p-value are calculated by non-parametric Wilcoxon signed rank test, results for whole curves comparisons are shown. (nonetheless, p-value of 2-way Anova is also significative, p=0.0002) Individual images for each mouse at different time points on the right. **(B)** Survival curves for mice treated with the aforementioned conditions. P-values have been determined by log-rank mantel-cox test. **(C)** Log2 fold change variations in frequencies of gRNAs targeting *MED12*, through different time points. variations are normalised to non-targeting guides and are calculated as average values for all sgRNA in the three donors. **(D)** Flow cytometry based differentiation profiling for *MED12* KO CAR-T cells (n=3) as compared to CTRL CAR-T cells (n=3) at the endpoint of production phase. T-scm (T stem cell memory) are defined as CD45RA+ and CD27+ t-cells. P-values are calculated with paired ratio t-tests.

Figure 7

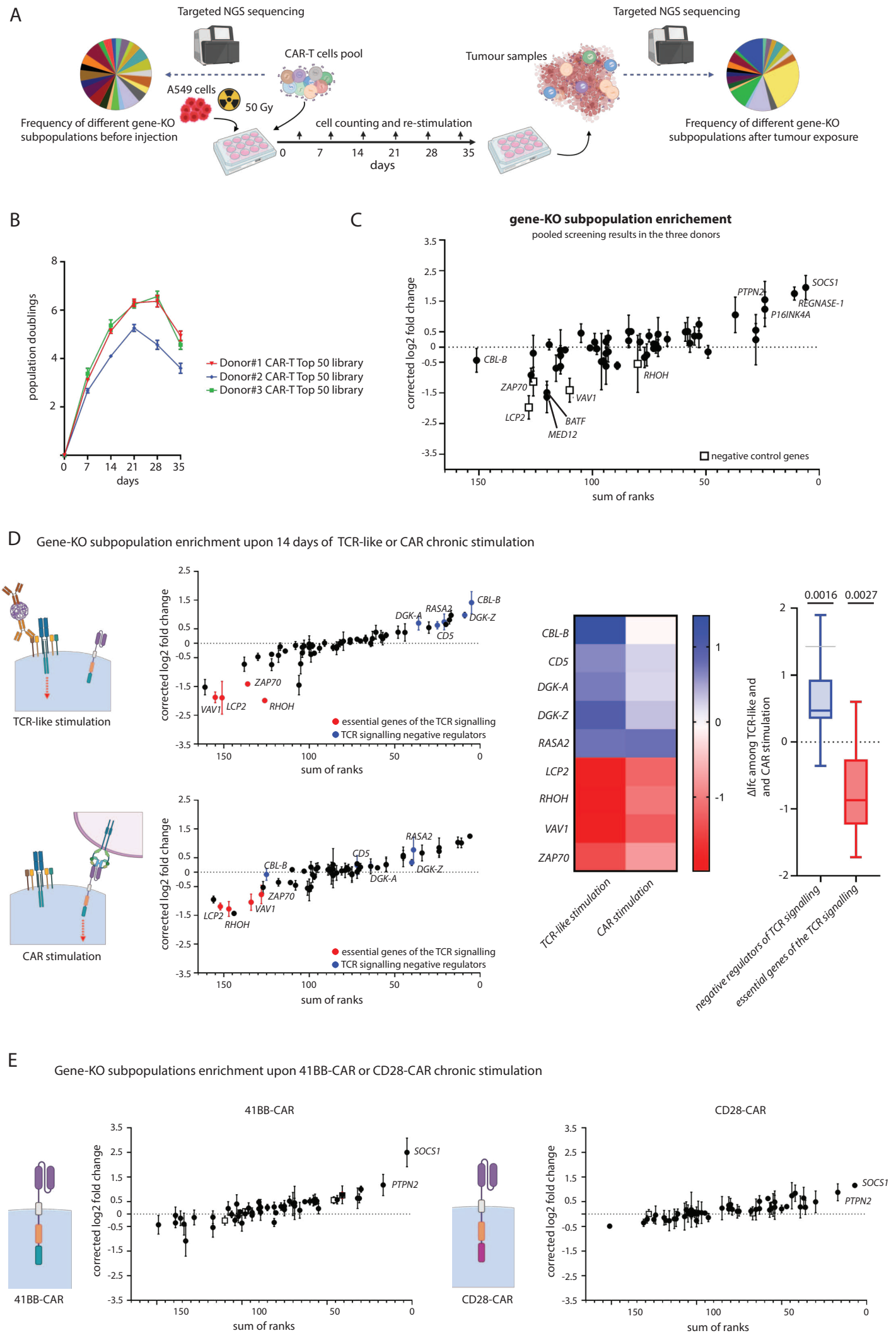
A
Targeted NGS sequencing
CAR-T cells pool
A549 cells
50 Gy
Frequency of different gene-KO subpopulations before injection
cell counting and re-stimulation
0 7 14 21 28 35
days
Tumour samples
Targeted NGS sequencing
Frequency of different gene-KO subpopulations after tumour exposure
B
population doublings
days
Donor#1 CAR-T Top 50 library
Donor#2 CAR-T Top 50 library
Donor#3 CAR-T Top 50 library
C
gene-KO subpopulation enrichement
pooled screening results in the three donors
corrected log2 fold change
sum of ranks
SOCS1
PTPN2
RNGNASE-1
P16INK4A
CBL-B
RHOH
ZAP70
VAV1
LCP2
BATF
MED12
negative control genes
D
Gene-KO subpopulation enrichment upon 14 days of TCR-like or CAR chronic stimulation
TCR-like stimulation
CAR stimulation
essential genes of the TCR signalling
TCR signalling negative regulators
CBL-B
DGK-A
RASA2
DGK-Z
CD5
ZAP70
VAV1
LCP2
RHOH
0.0016
0.0027
ΔIfc among TCR-like and and CAR stimulation
negative regulators of TCR signalling
essential genes of the TCR signalling
E
Gene-KO subpopulations enrichment upon 41BB-CAR or CD28-CAR chronic stimulation
41BB-CAR
CD28-CAR
SOCS1
PTPN2

Figure 7 Application of the screening *in vitro,* for the study of the impact of signalling differences on gene-KO strategies efficacy: **(A)** Schematics of the experiment **(B)** CAR-T cell proliferation curve as determined by cell counting, 3 replicates for each of 3 donors derived CAR-T cells Donor#1, Donor#2, Donor#3. **(C)** Overall results pooling three independent screenings, log2 fold change for each gene is calculated as average of these values from each screening. Sum of rank value is determined as sum of the rankings assigned by MAGeCK alpha-RRA algorithm for each gene in the three screenings. gene-ko subpopulation frequency variations are compared at the endpoint of the experiment, 35 days, vs in starting products. **(D)** (left) Screening results from three different experiments in which CAR-T cells either were stimulated by anti-CD3/CD28 polymers or irradiated tumor cells, every 3 to 5 days for 14 days, to assess mainly proliferation effects. Gene-ko subpopulation proportions are compared at the endpoint of the experiment vs in starting products. (middle) Heatmap representation of log2 fold change variation for genes either essential to or negatively regulating the TCR pathway. (right) Overall difference in log2 fold change in frequency of CAR-T cells carrying mutation in negative regulators of the TCR pathway and essential genes of this pathway. Variations in CAR-T cells stimulated with anti-CD3/CD28 polymers compared to variations in CAR stimulated CAR-T cells. TCR-like stimulation lead to significantly increased variations for such groups of genes, in both directions. **(E)** Overall results pooling three independent screenings, either with (left) 41BB CAR-T cells or (right) CD28 CAR-T cells. Log2 fold change for each gene is calculated as average of these values from each screening. Sum of rank value is determined as sum of the rankings assigned by MAGeCK alpha-RRA algorithm for each gene in the three screenings. Gene-ko subpopulation frequency variations are compared at the endpoint of the experiment, 35 days, vs in starting products.

Figure 8

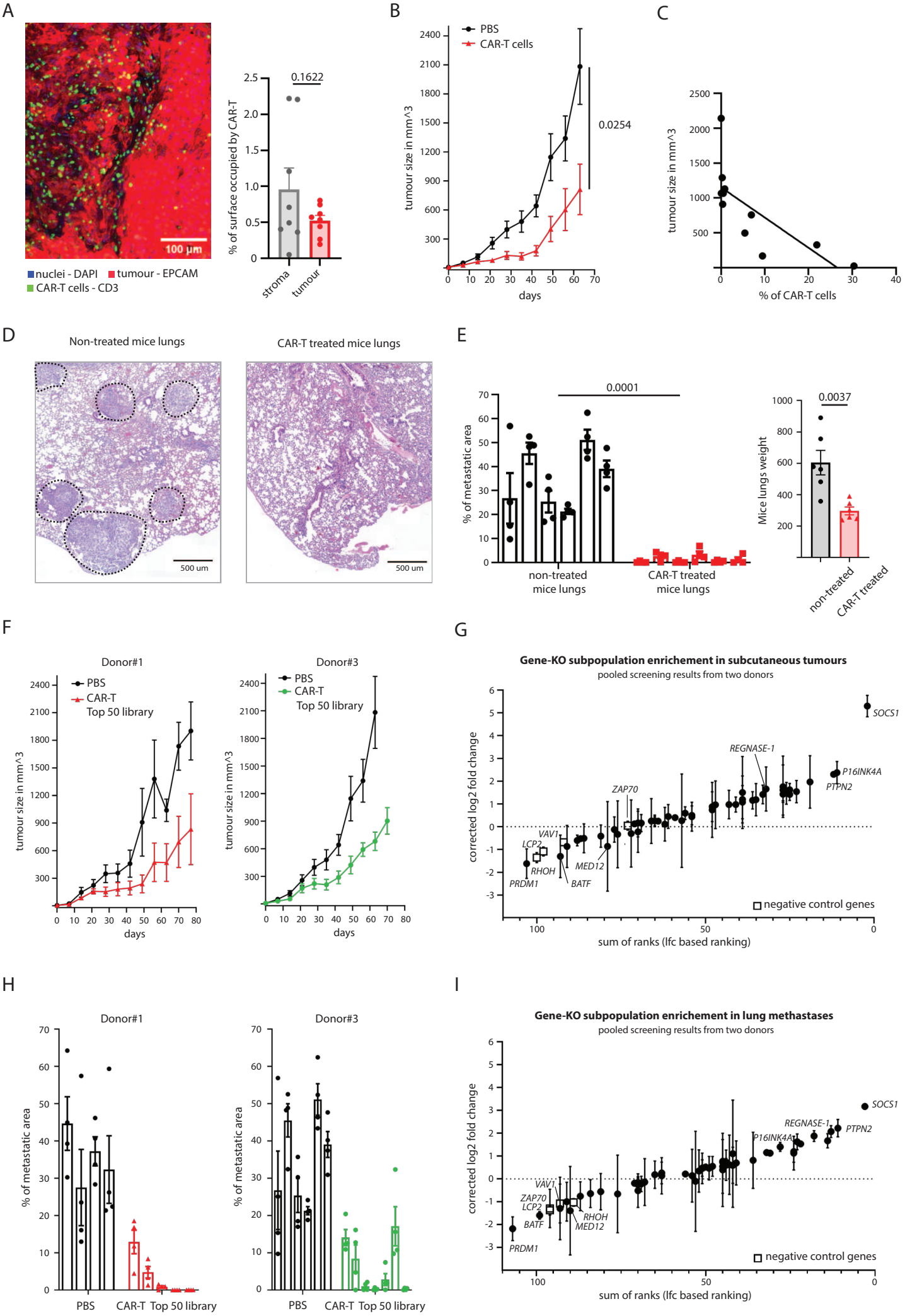
A
100 µm
nuclei - DAPI
tumour - EPCAM
CAR-T cells - CD3
% of surface occupied by CAR-T
0.1622
stroma
tumour
B
PBS
CAR-T cells
tumour size in mm^3
0.0254
days
C
tumour size in mm^3
% of CAR-T cells
D
Non-treated mice lungs
CAR-T treated mice lungs
500 um
E
% of metastatic area
0.0001
non-treated mice lungs
CAR-T treated mice lungs
Mice lungs weight
0.0037
non-treated
CAR-T treated
F
Donor#1
Donor#3
PBS
CAR-T
Top 50 library
tumour size in mm^3
days
G
Gene-KO subpopulation enrichment in subcutaneous tumours
pooled screening results from two donors
corrected log2 fold change
SOCS1
REGNASE-1
P16INK4A
PTPN2
ZAP70
VAV1
LCP2
RHOH
MED12
PRDM1
BATF
negative control genes
sum of ranks (lfc based ranking)
H
Donor#1
Donor#3
% of metastatic area
PBS
CAR-T
Top 50 library
I
Gene-KO subpopulation enrichment in lung methastases
pooled screening results from two donors
corrected log2 fold change
SOCS1
REGNASE-1
PTPN2
P16INK4A
VAV1
ZAP70
LCP2
BATF
RHOH
MED12
PRDM1
negative control genes
sum of ranks (lfc based ranking)

Figure 8. ***SOCS1* KO outperforms other gene inactivation strategies in the *In vivo* screening in the subcutaneous tumor model**: **(A)** Immunofluorescence microscopy image of A549 cells subcutaneous tumor, with CAR-T infiltrate and quantification of CAR-T cells infiltration in tumor mass vs stroma (n=8 tumor slices images) **(B)** Tumor growth curve, assessed by caliper measurements, in mice receiving mock solution (n=5) or treated with 7*10^6 cells(n=5). p-values are calculated by two-ways ANOVA test. **(C)** Negative correlation among tumor mass, and % of CAR-T cells in mice tumor at the experiment endpoint. **(D)** Haematoxylin-Eosin staining of mice lung slices, showing metastatic burden respectively in mice treated with mock or CAR-T cells. **(E)** Machine learning quantification of metastatic area in subcutaneous tumor bearing mice, treated with mock or CAR-T cells. (respectively n=20 and 24 images were used for calculation) p-value is calculated by unpaired t-test. **(F)** Tumor growth curve, assessed by caliper measurements, in mice receiving mock solution (n=5 for both experiments) or treated with modified CAR-T cells 5*10^6 cells. On the left an experiment with donor Donor#1 CAR-T cells (n=5), on the right the same with donor Donor#3 CAR-T cells (n=6). **(G)** Overall results pooling two independent screenings, log2 fold change for each gene is calculated as average of these values from each screening. Sum of rank is determined as sum of LFC based ranking in each experiment. gene-ko subpopulation frequency variations are compared at the endpoint of the experiment, 70 to 77 days, vs starting products. **(H)** Machine learning based quantification of metastatic area in subcutaneous tumor bearing mice treated or not with CAR-T cells. (n=16 and 20 images for mock and CAR-T treated mice for Donor#1 experiment, n=24 and 24 for the Donor#3 experiment) **(I)** Overall results pooling two independent screenings in the lungs of mice with subcutaneous tumor, log2 fold change for each gene is calculated as average of these values from each screening. Sum of rank value is determined as sum of LFC based ranking in each experiment. Gene-ko subpopulation frequency variations are compared at the endpoint of the experiment, 70 to 77 days, vs starting products.

Figure 9

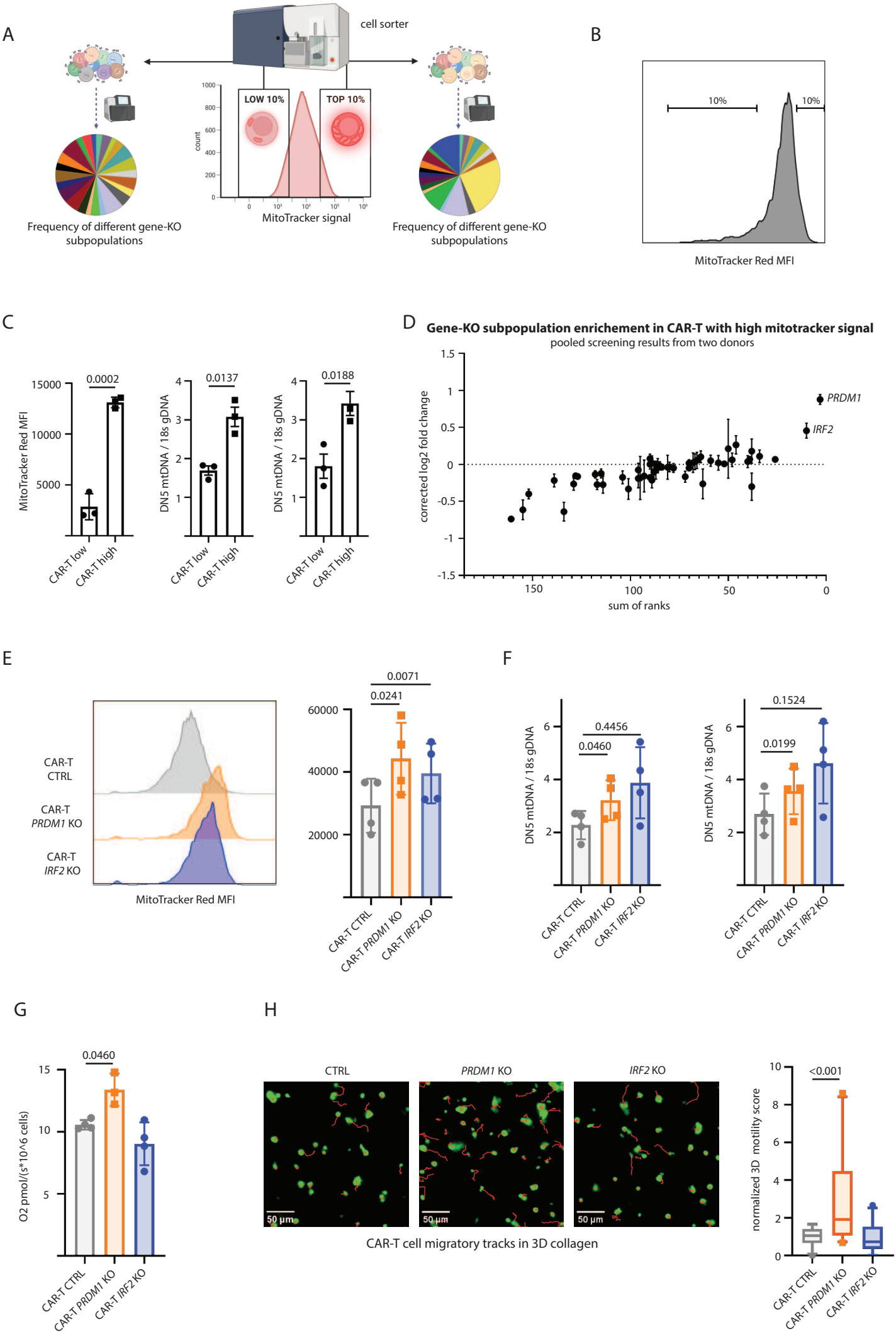
A
cell sorter
LOW 10%
TOP 10%
count
MitoTracker signal
Frequency of different gene-KO subpopulations
Frequency of different gene-KO subpopulations
B
10%
10%
MitoTracker Red MFI
C
MitoTracker Red MFI
0.0002
DN5 mtDNA / 18s gDNA
0.0137
DN5 mtDNA / 18s gDNA
0.0188
CAR-T low
CAR-T high
D
Gene-KO subpopulation enrichement in CAR-T with high mitotracker signal
pooled screening results from two donors
corrected log2 fold change
PRDM1
IRF2
sum of ranks
E
CAR-T CTRL
CAR-T PRDM1 KO
CAR-T IRF2 KO
MitoTracker Red MFI
0.0071
0.0241
F
DN5 mtDNA / 18s gDNA
0.4456
0.0460
0.1524
0.0199
CAR-T CTRL
CAR-T PRDM1 KO
CAR-T IRF2 KO
G
O2 pmol/(s*10^6 cells)
0.0460
H
CTRL
PRDM1 KO
IRF2 KO
50 µm
CAR-T cell migratory tracks in 3D collagen
normalized 3D motility score
<0.001

Figure 9. **Screening application to study the improvement of CAR-T cells mitochondrial mass, respiratory and migratory capacity**: **(A)** Schematics of the experiment. **(B)** Exemplary gating for sorting on MitoTracker red signal levels, top 10% and bottom 10% cells have been selected. **(C)** Mitochondrial mass quantification by qPCR measurement of mtDNA copies as compared to genome copies in sorted CAR-T cells. Mitochondrial genes ND1 and ND5 were used for mitochondrial DNA, gene 18s was used for genomic DNA. (n=3 for group) p-values are calculated with one-way Anova test. **(D)** Screening results from three different experiments. gene-ko subpopulation proportions are compared in high vs low MitoTracker signal cells. **(E)** MitoTracker signal levels for CAR-T cells KO for genes *PRDM1* or *IRF2* compared to CTRL ones.(n=4 for group) p-values are calculated with one-way Anova test **(F)** Mitochondrial mass quantification by qPCR measurement of mtDNA copies as compared to genome copies for CAR-T cells KO for genes *PRDM1* or *IRF2* compared to CTRL ones. (n=4 for group) p-values are calculated with one-way Anova test. **(G)** Maximal respiratory capacity as assessed by OROBOROS measurements. (n=3 for *PRDM1* KO, n=4 for CTRL and *IRF2* KO CAR-T) p-values are calculated with one-way Anova test. **(H)** Exemplary migration tracks of CTRL, *PRDM1* KO or *IRF2* KO CAR-T cells in 3D collagen. **(I)** Normalized 3D motility score of CTRL, *PRDM1* KO or *IRF2* KO CAR-T cells. Such score is calculated as product of speed of migrating cell, distance covered and % of actually migrating cells. (n=23 videos) p-values are calculated with one-way Anova on ranks test, with Tukey post-hoc correction.

Supplementary figure 1

A

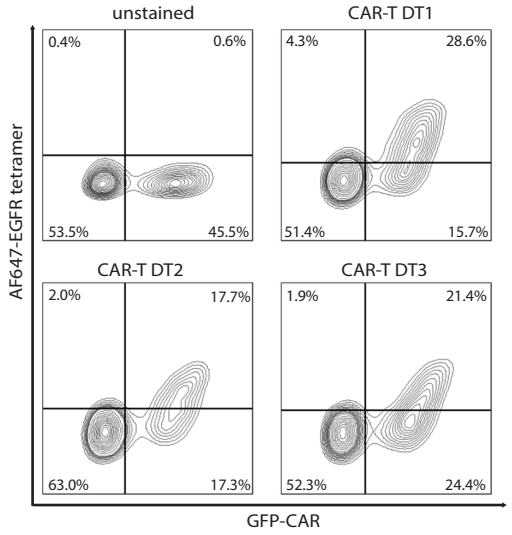

B

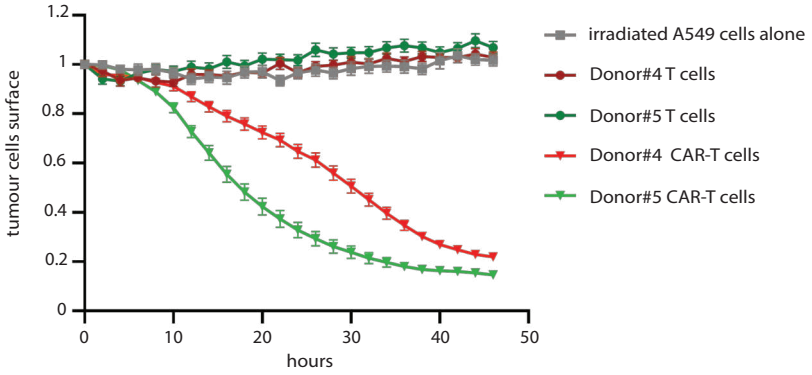

C

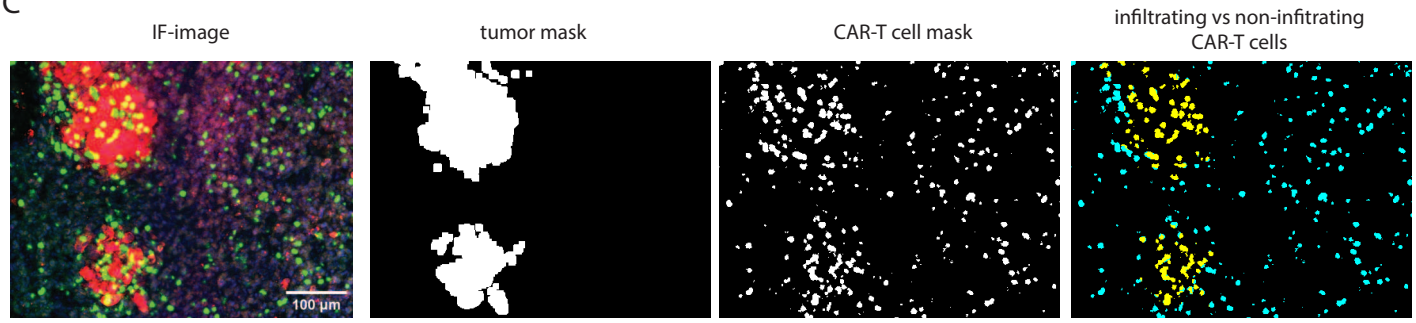

D

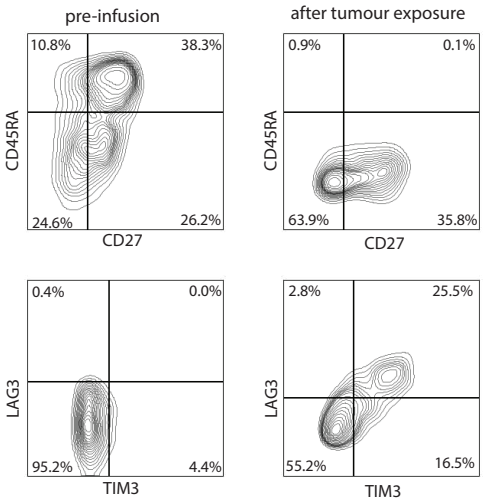

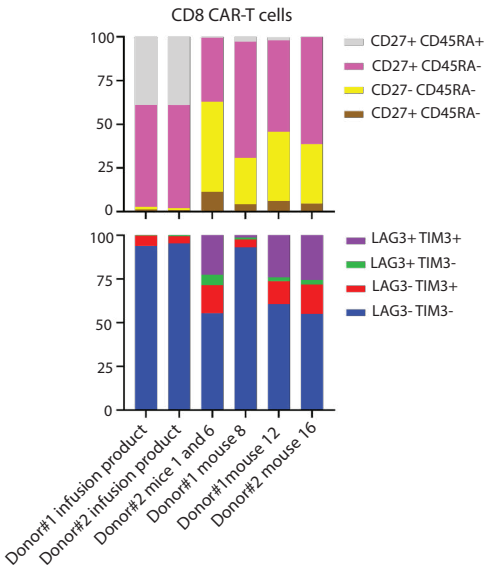

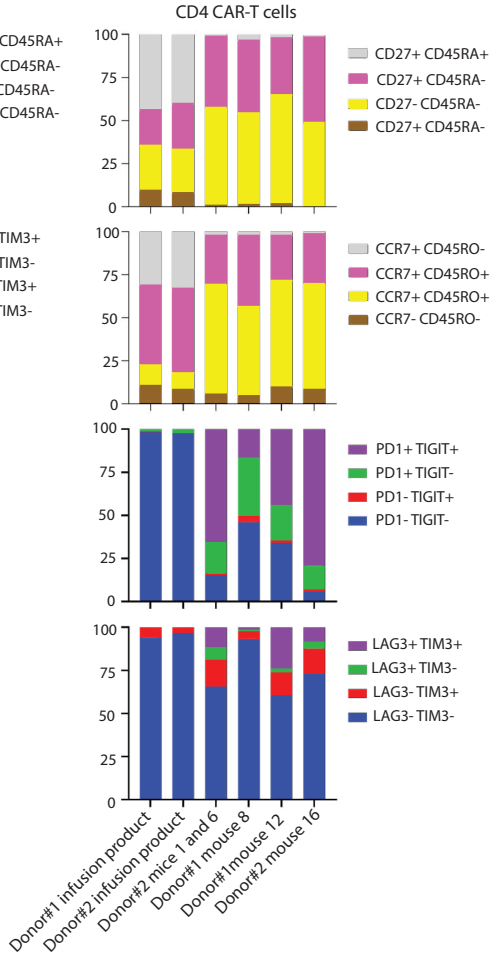

Supplementary Figure 1. Validation of CAR-T cells specificity and of the orthotopic lung tumour model: **(A)** CAR-T cells binding with biotin-EGFR recombinant protein conjugated in tetramers with A647-streptdadivin. **(B)** CAR-T cells mediated killing of A549 cells as assessed as reduction of mCherry+ area, measured by Incucyte imaging. **(D)** CAR-T cells infiltration in tumour islets quantification strategy, from left to right images of different masks used, and merged image of CAR-T cells colocalizing (yellow) or not (cyan) with the EpCAM mask. **(E)** Phenotypical characterisation of CAR-T cells by flow cytometry. We compared CAR-T cells from infusion products and CAR-T cells recovered from mice which received the 5*10^6 dose after long term exposure to tumour *in vivo*.

Supplementary figure 2

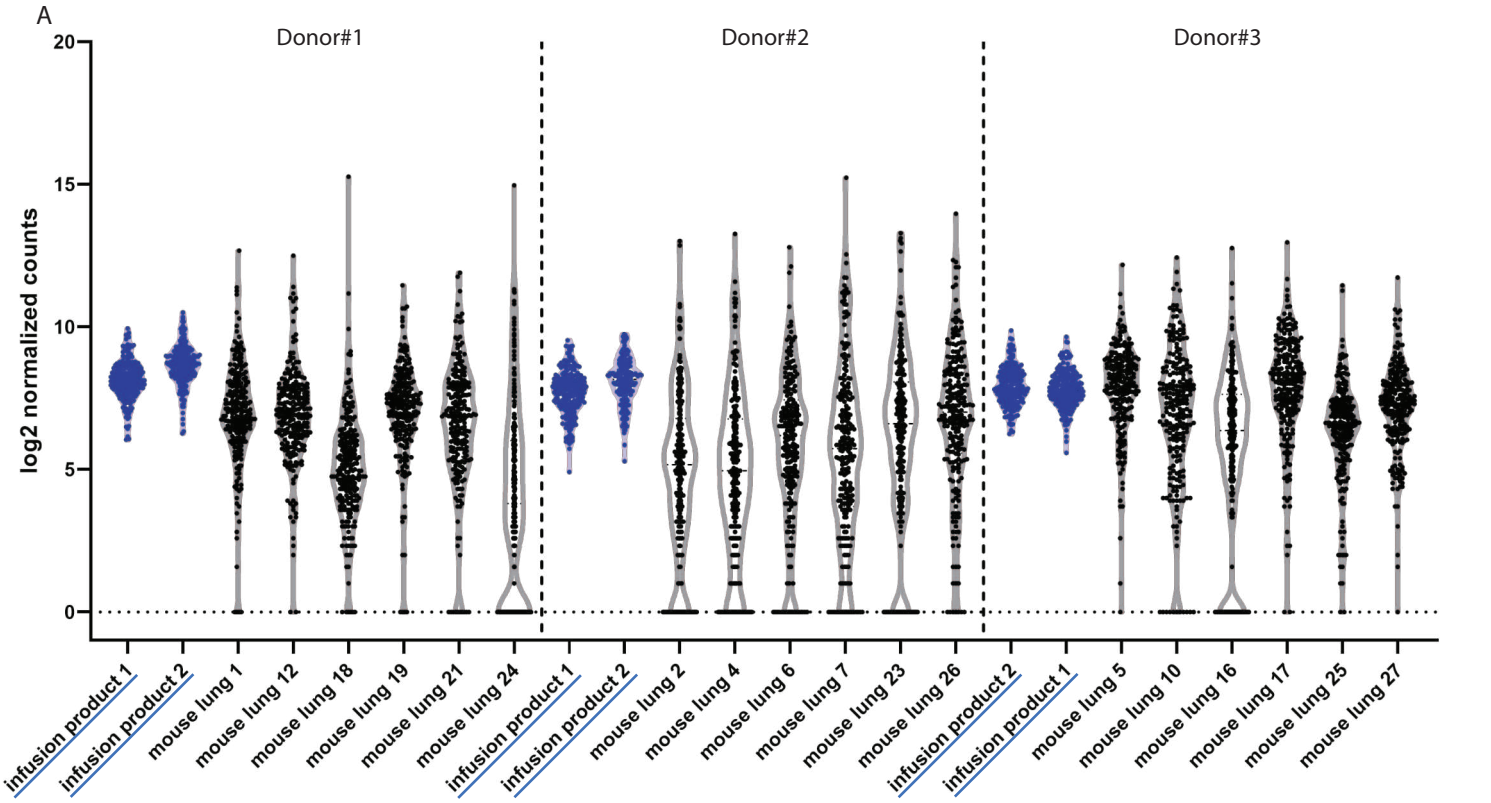

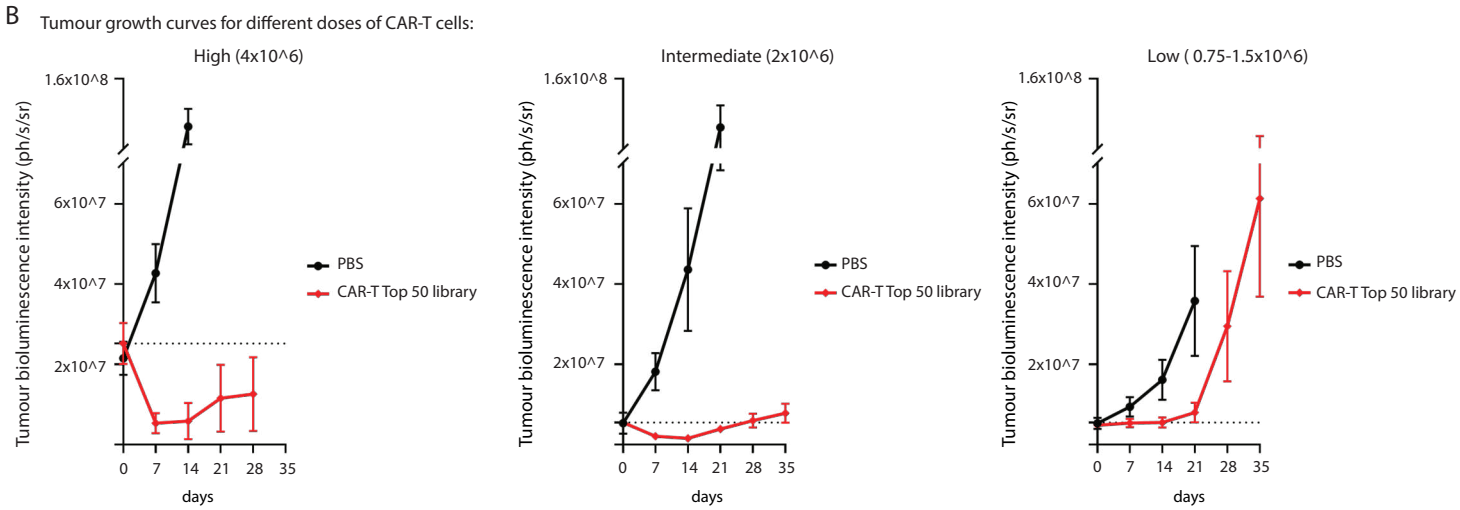

Supplementary figure 2. Additional details on the *in vivo* screening assays: (**A**) log2 counts of sgRNA in CAR-T cells from the three different donors, compared in mice lungs at the endpoint of the experiment vs in infusion products. For CAR-T cells from donor#1 data from mice 19 and 24, that died before the expected endpoint, (among 21 and 28 days) were included too. For CAR-T cells from donor#3, DNA sample from mouse 11 could not be treated. (**B**) Tumour growth curves as determined by bioluminescence for mice in different experiments on the same donor CAR-T cells, Donor#3. Mice first received 10*10^6 A549 cells in the first experiment and 4*10^6 In both the other ones. In the first experiment mice are treated either with excipient (n=5) or 4*10^6 CAR-T modified with our Top 50 library lentivirus bank (n=5), in the second experiment they are treated either with excipient (n=5) or 2*10^6 CAR-T modified with our Top 50 library lentivirus bank (n=5), in the third experiment they are treated either with excipient (n=5) or 0.75-1.5*10^6 CAR- T modified with our Top 50 library lentivirus bank (respectively n=4 and n=4),

Supplementary figure 3

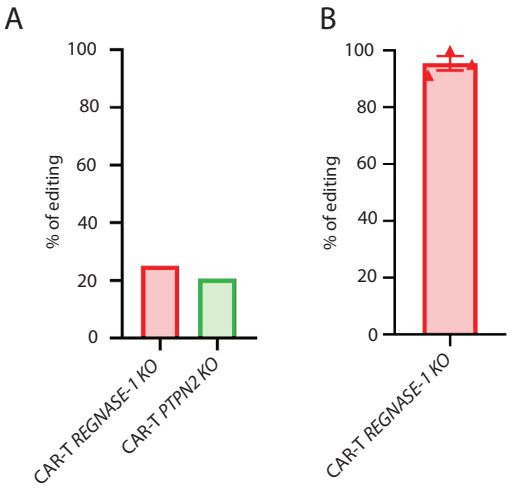

Supplementary figure 3, Editing validation for *PTPN2* KO and *REGNASE-1* KO in different experiments: (**A**) quantification of *REGNASE-1* and *PTPN2* gene editing in CAR-T cells used for the validation in vivo experiments, as evaluated by proportion of modified genomic sequences upon knock out, determined through sanger sequencing and deconvolution analysis of chromatograms files. (**B**) Quantification of *REGNASE-1* gene editing in CAR-T cells used for the in vitro suicide gene experiment, as evaluated by proportion of modified genomic sequences upon knock out, determined through sanger sequencing and deconvolution analysis of chromatograms files. (n=3) To maximize editing efficiency, we used a double gRNA approach with recently described highly effective *REGNASE-1* targeting sgRNA sequences.

Supplementary figure 4

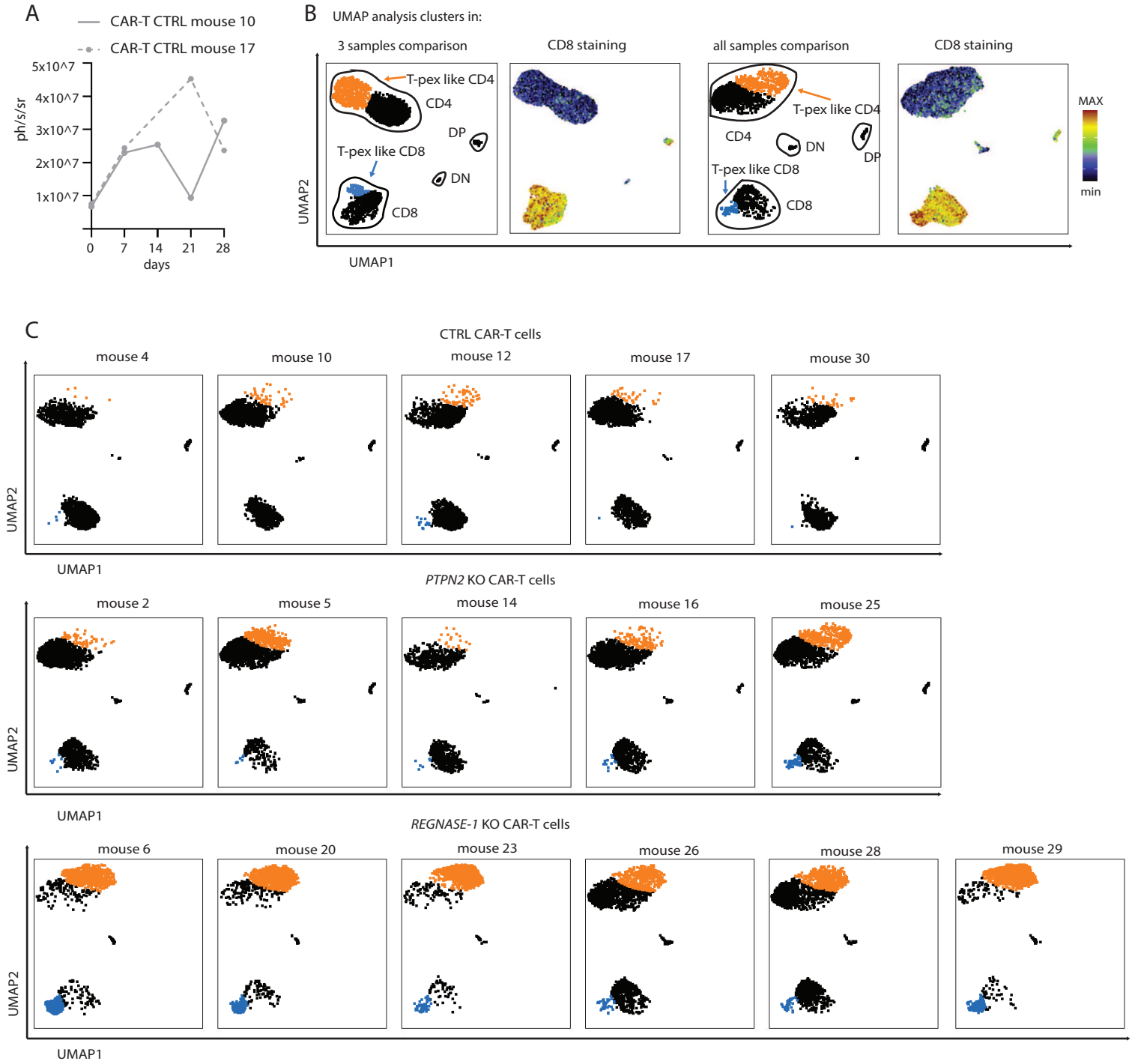

Supplementary Figure 4. Detailed sample-by-sample clustering analysis of CyTOF data: (**A**) Tumour growth curve in mice 10 and 17, these mice were excluded from the tumour control comparison experiment, because of excessive tumour burden. These mice were treated with a higher dose of CTRL CAR-T cells, 2*10^6 and were used as additional controls exclusively for the CyTOF experiment. (**B**) Comparison of UMAP analysis of CyTOF data from CAR-T cells in lung tumour samples at the endpoint of the experiment, either confronting clustering in the analysis with three exemplary samples, as in the main figure 5, or including all samples in the analysis. (**C**) UMAP analysis of CyTOF data from CAR-T cells in lung tumour samples at the endpoint of the experiment, in this analysis all samples were included.

Supplementary figure 5

A

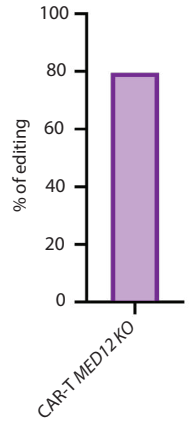

B

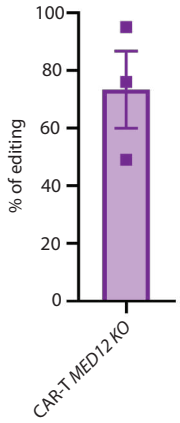

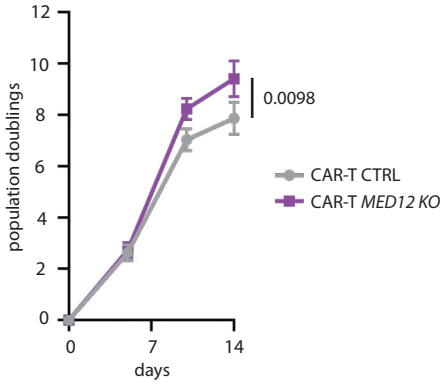

C

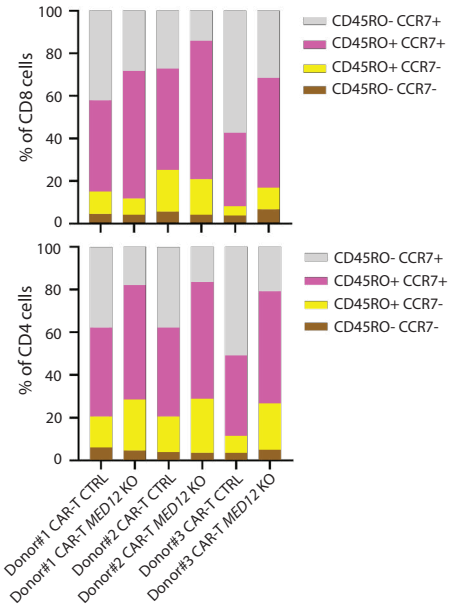

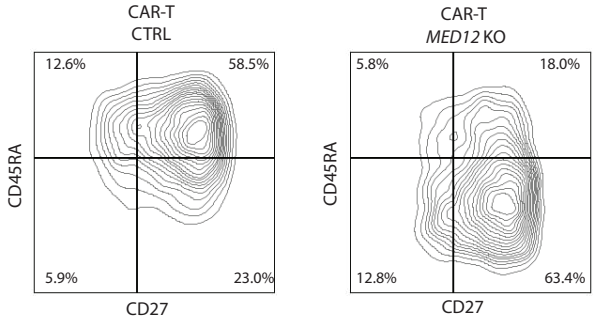

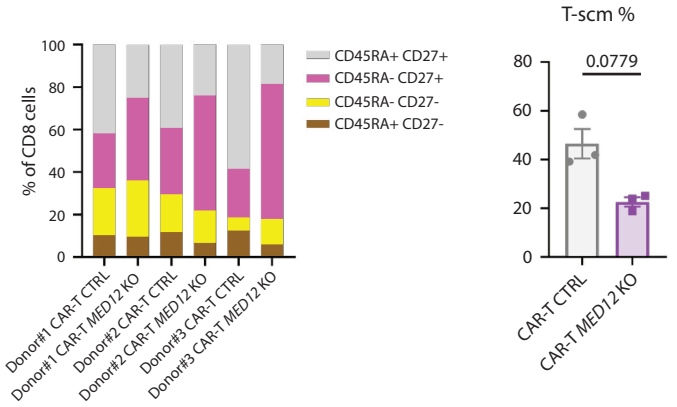

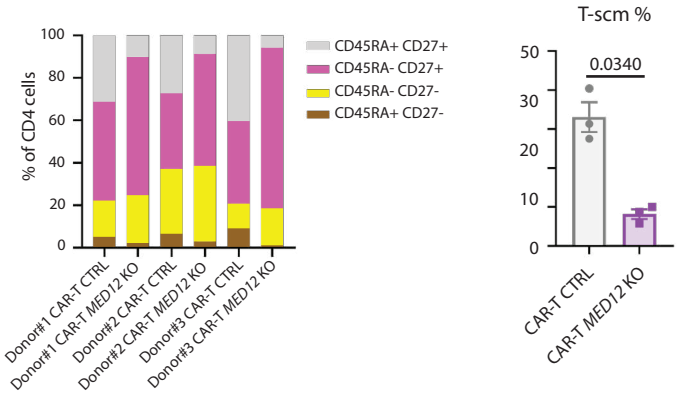

Supplementary figure 5. Validation of *MED12* editing in different experiments and additional characterisation of *MED12* KO CAR-T cells: **(A)** quantification of *MED12* gene editing in CAR-T cells used for the validation in vivo experiment, as evaluated by proportion of modified genomic sequences upon knock out, determined through sanger sequencing and deconvolution analysis of chromatograms files. **(B)** (left) Quantification of *MED12* gene editing in CAR-T cells used for in vitro characterisation experiments, as evaluated by proportion of modified genomic sequences upon knock out, determined through sanger sequencing and deconvolution analysis of chromatograms files. (right) *In vitro* proliferation during production phase for *MED12* KO CAR-T cells as compared to CTRL CAR-T cells (n=3) **(D)** Flow cytometry-based differentiation profiling for *MED12* KO CAR-T cells as compared to CTRL CAR-T cells at the endpoint of production phase. (n=3 per group) T-scm (T stem cell memory) are here defined as CD45RA+ and CD27+ t-cells, to confirm data from the main figure by a different staining. P-values are calculated with unpaired t-tests.

Supplementary figure 6

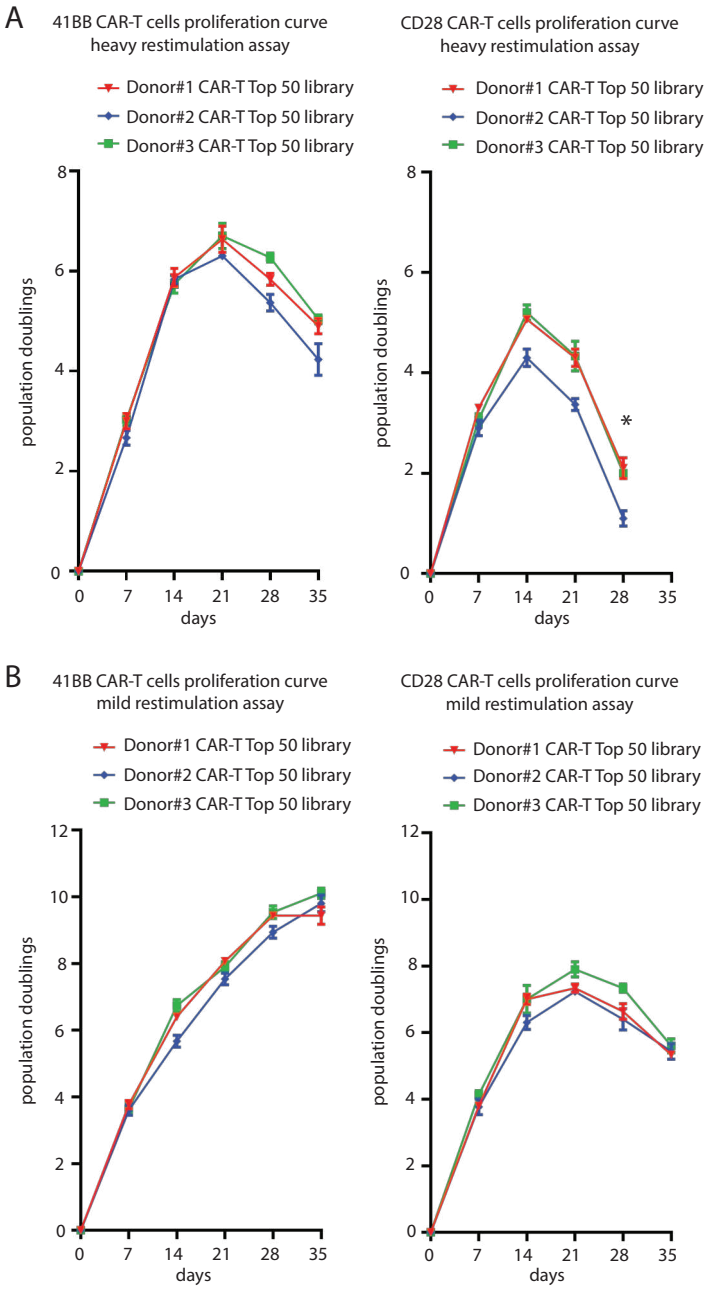

Supplementary figure 6. 41BB-CAR-T and CD28-CAR-T cells proliferation curves in restimulation assays: **(A)** 41BB-CAR-T and CD28-CAR-T cells proliferation curve, expressed in population doublings, in the heavy restimulation assay. Numbers are determined by Trypan Blue corrected cell counting, we cultured 3 replicates for each of 3 donors derived CAR-T cells Donor#1, Donor#2, Donor#3. For the CD28 condition, (* at 28 days we could not detect enough live cells to relaunch the co-culture.) **(B)** 41BB-CAR-T and CD28-CAR-T cells proliferation curve, expressed in population doublings, in the mild restimulation assay. Numbers are determined by Trypan Blue corrected cell counting, we cultured 3 replicates for each of 3 donors derived CAR-T cells Donor#1, Donor#2, Donor#3.

Supplementary figure 7

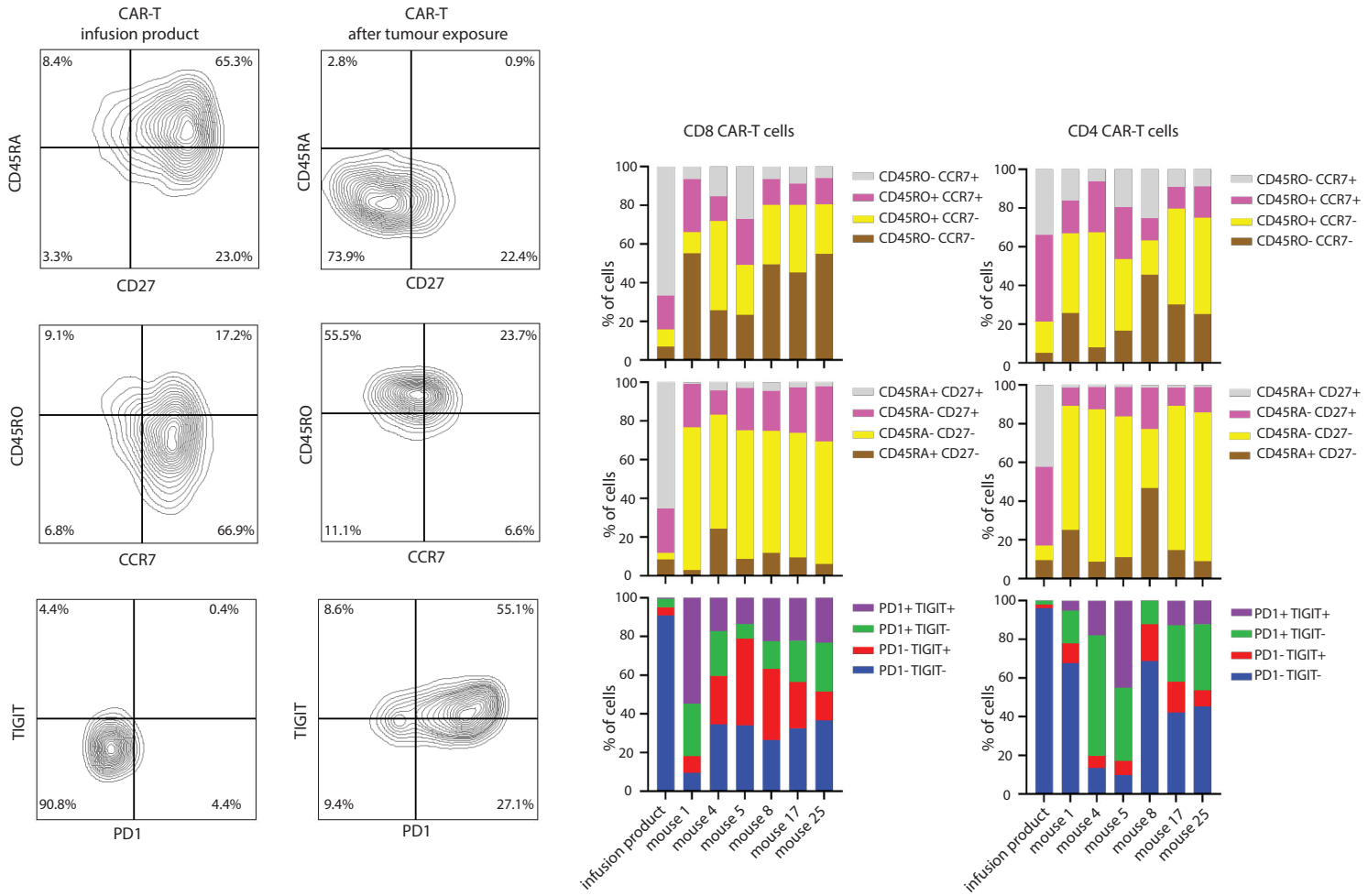

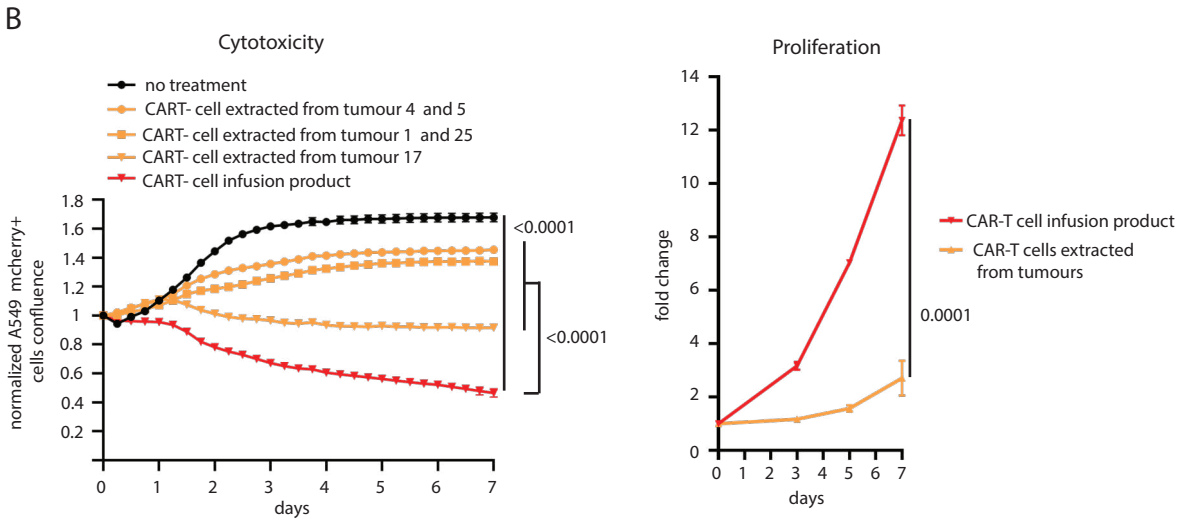

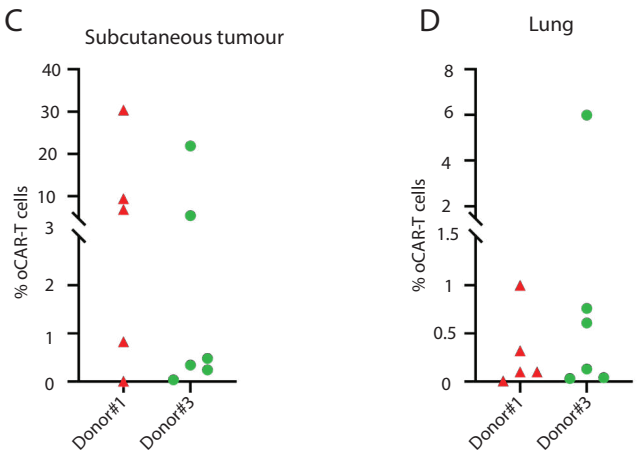

Supplementary figure 7. Characterization of the A549 subcutaneous tumour model: **(A)** Phenotypical characterisation of CAR-T cells by flow cytometry. We compared CAR-T cells from infusion products and CAR-T cells recovered from mice subcutaneous tumours which received 5*10^6 CAR-T cells, after long term exposure to tumour *in vivo*. **(B)** Functional characterisation of compared CAR-T cells from infusion products and CAR-T cells recovered from mice. Cytotoxic capacity was assessed by calculating surface reduction of mCherry+ tumour cells when co-cultured with CAR-T cells. Proliferation capacity was assessed by cell counting upon 7 days after anti-CD3/C28 stimulation. P-values are calculated by two-ways ANOVA test, results for final time point comparisons are shown. **(C)** CAR-T cells detection in mice subcutaneous tumours and **(D)** lungs by flow cytometry, for Donor#1 (n=5) and Donor#3 (n=6)

Supplementary figure 8

A

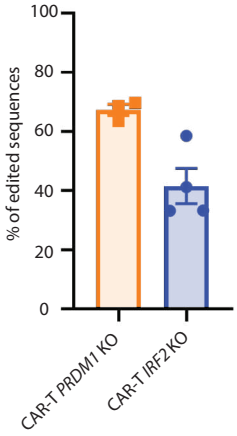

Supplementary figure 8. *PRDM1* and *IRF2* gene editing validation: **(A)** Quantification of *PRDM1* and *IRF2* gene editing in CAR-T cells used for all the in vitro experiments, as evaluated by proportion of modified genomic sequences upon knock out, determined through sanger sequencing and deconvolution analysis of chromatograms files. (n=4 for group)